Article

Cell

Integrated Control of Predatory Hunting by the Central Nucleus of the Amygdala

Graphical Abstract

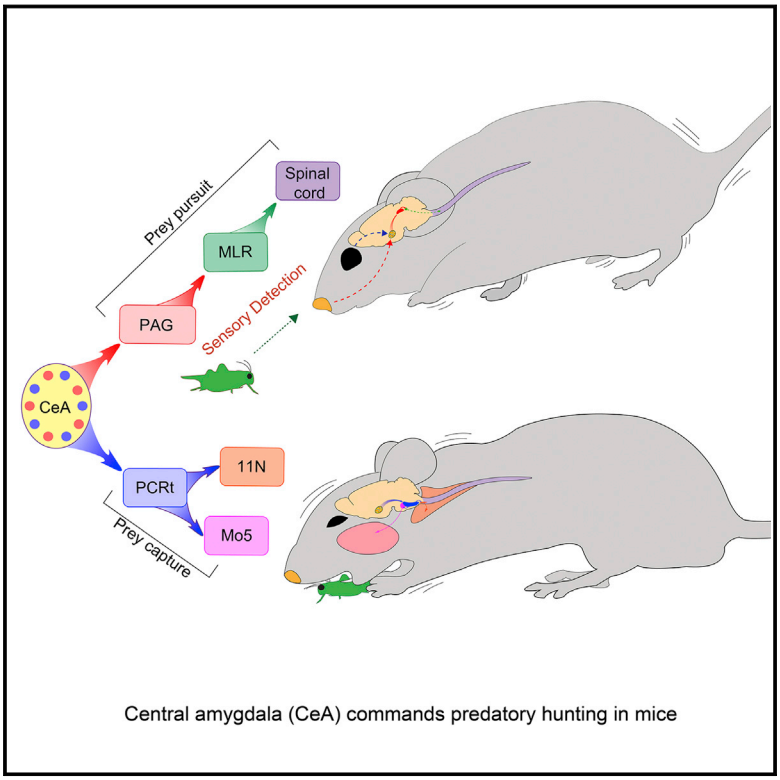

Central amygdala (CeA) commands predatory hunting in mice

Authors

Wenfei Han, Luis A. Tellez, Miguel J. Rangel, Jr., ..., Sara J. Shammah-Lagnado, Anthony N. van den Pol, Ivan E. de Araujo

Correspondence

iaraujo@jbpierce.org

In Brief

Two neuronal pathways originating in the central amygdala coordinate distinct behaviors necessary for efficient predatory hunting: the ability to pursue a prey and deliver fatal bites upon capture.

Highlights

- Stimulation of central amygdala (CeA) elicited hunting of live and artificial prey
- CeA projections to the reticular formation (PCRt) control biting attacks
- CeA projections to periaqueductal gray (PAG) control locomotion during pursuit
- CeA integrates craniofacial and locomotor modules during goal-directed behavior

Han et al., 2017, Cell *168*, 311–324
January 12, 2017
http://dx.doi.org/10.1016/j.cell.2016.12.027

CellPress

Cell

Integrated Control of Predatory Hunting by the Central Nucleus of the Amygdala

Wenfei Han,[1,2,3] Luis A. Tellez,[1,2] Miguel J. Rangel, Jr.,[1,2,4] Simone C. Motta,[4] Xiaobing Zhang,[5] Isaac O. Perez,[1] Newton S. Canteras,[4] Sara J. Shammah-Lagnado,[6] Anthony N. van den Pol,[5] and Ivan E. de Araujo[1,2,7,8,*]
[1]The John B Pierce Laboratory, New Haven, CT 06519, USA
[2]Department of Psychiatry, Yale University School of Medicine, New Haven, CT 06519, USA
[3]School & Hospital of Stomatology, Tongji University, Shanghai Engineering Research Center of Tooth Restoration and Regeneration, Shanghai 200072, China
[4]Department of Anatomy, Biomedical Sciences Institute, University of São Paulo, São Paulo 05508, Brazil
[5]Department of Neurosurgery, Yale University School of Medicine, New Haven, CT 06519, USA
[6]Department of Physiology and Biophysics, Biomedical Sciences Institute, University of São Paulo, São Paulo 05403, Brazil
[7]Department of Cellular and Molecular Physiology, Yale University School of Medicine, New Haven, CT 06511, USA
[8]Lead Contact
*Correspondence: iaraujo@jbpierce.org
http://dx.doi.org/10.1016/j.cell.2016.12.027

SUMMARY

Superior predatory skills led to the evolutionary triumph of jawed vertebrates. However, the mechanisms by which the vertebrate brain controls predation remain largely unknown. Here, we reveal a critical role for the central nucleus of the amygdala in predatory hunting. Both optogenetic and chemogenetic stimulation of central amygdala of mice elicited predatory-like attacks upon both insect and artificial prey. Coordinated control of cervical and mandibular musculatures, which is necessary for accurately positioning lethal bites on prey, was mediated by a central amygdala projection to the reticular formation in the brainstem. In contrast, prey pursuit was mediated by projections to the midbrain periaqueductal gray matter. Targeted lesions to these two pathways separately disrupted biting attacks upon prey versus the initiation of prey pursuit. Our findings delineate a neural network that integrates distinct behavioral modules and suggest that central amygdala neurons instruct predatory hunting across jawed vertebrates.

INTRODUCTION

The emergence of articulated jaws was a major event in vertebrate evolution. The reconfiguration of the vertebrate head promoted the transition from filter feeding to active predation, eventually placing jawed predators at the top of the food chain (Gans and Northcutt, 1983; Kuratani, 2012; Mallatt, 2008). This morphological transformation was met with the development of novel neural networks capable of coordinating craniofacial and locomotor systems during active hunting (Gans and Northcutt, 1983). Dissecting the neural circuitry of predation may, therefore, provide unique insights into the evolution of vertebrate sensorimotor systems (Borghuis and Leonardo, 2015; Catania, 2012).

We hypothesized a role for the central nucleus of the amygdala (CeA) in predatory hunting. The hypothesis is based on the finding that hunting prey produces greater activation of CeA neurons than surges in food intake (Comoli et al., 2005). Moreover, CeA projects densely to brainstem premotor circuits involved in craniofacial control (Shammah-Lagnado et al., 1992; Swanson and Petrovich, 1998; Van Daele et al., 2011). Accordingly, we combined cell-specific manipulations with an ethological assay (cricket hunting, Butler, 1973; Nikulina, 1981) to investigate the role of CeA in promoting predation in mice.

RESULTS

The Central Nucleus of the Amygdala Activates Craniofacial Musculatures and Promotes Predatory Hunting

Restricted transfection of the light-sensitive depolarizing *Channelrhodopsin2* (ChR2, Madisen et al., 2012) to the central nucleus of the amygdala (CeA) was achieved via stereotaxic injections of the *Cre*-inducible viral construct AAV-EF1a-DIO-hChR2(H134R)-EYFP into the CeA of VGat-ires-*Cre* mice (Figure 1A; for details on all brain injections see STAR Methods; Tables S1–S8). Anatomical and electrophysiological analyses of EYFP-expressing terminals confirmed the specificity of the *Cre*-dependent approach (Figures 1B and 1C and S1A–S1G; Swanson and Petrovich, 1998; Van Daele et al., 2011).

Coordinated action involving the neck and the jaw characterizes successful prey capturing in vertebrates (Finlay et al., 1980; Montuelle et al., 2009; Wainwright et al., 2008). We thus tested the ability of CeA neurons to concurrently control cervicalmandibular muscles. Optogenetic stimulation of CeA revealed a short-latency (<100 ms) co-activation of the masseter and trapezius muscles upon laser activation (Figures 1D–1F). When a non-edible item was placed in the cage, laser activation caused the otherwise indifferent mice to immediately assume a "capture-like" body posture and seize the object, which was then held with the forepaws and bitten. Behavior was interrupted immediately upon laser deactivation (Movie S1). Consistently, by employing the cricket-hunting paradigm (Butler, 1973; Finlay

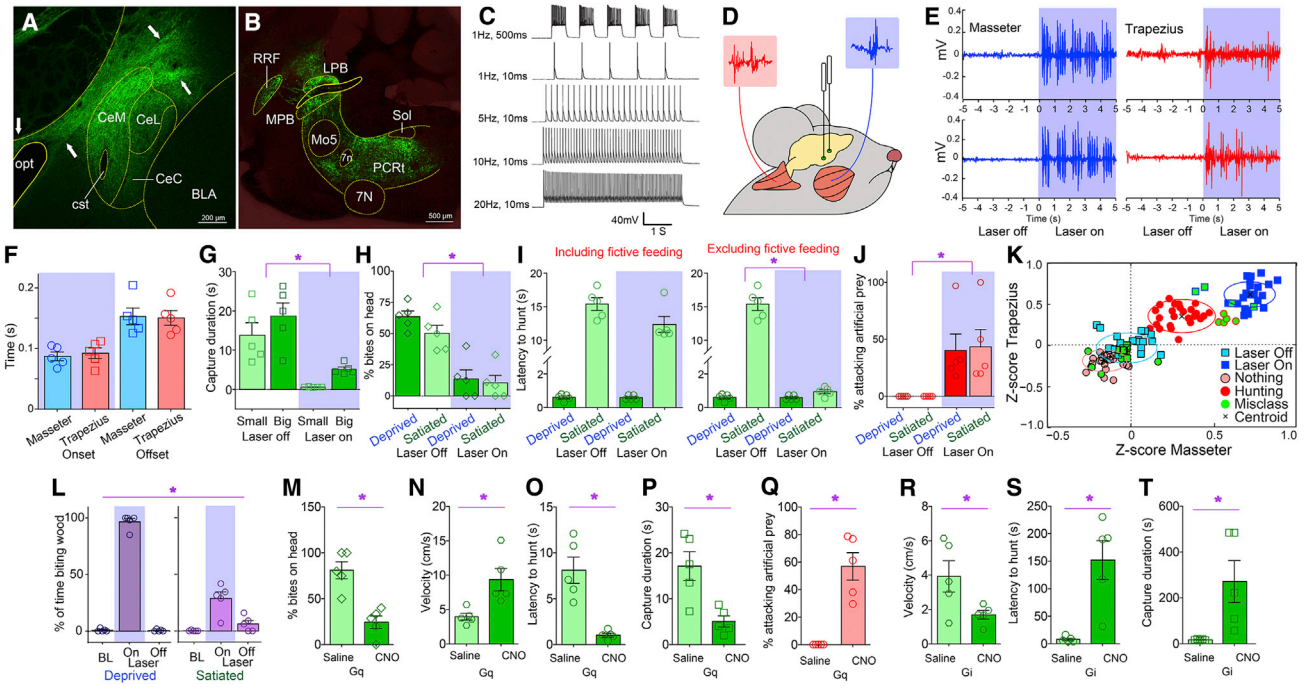

Figure 1. Central Amygdala Activates Craniofacial Musculatures and Promotes Predatory Hunting

(A) Coronal section illustrating *Cre*-dependent ChR2 expression in CeA of VGat-ires-Cre mice. Arrows indicate expression of the ChR2-fused fluorophore on projection axons originating in CeM. BLA, basolateral amygdala; CeM/CeL, CentroMedial/CentroLateral amygdala; opt, optic tract; cst, *stria terminalis*, commissural component.

(B) Sagittal section shows EYFP-expressing terminals in brainstem nuclei involved in craniofacial motor control. 7N, (Facial) motor nucleus VII; 7n, facial nerve tract; Mo5, (trigeminal) motor nucleus V; LPB/MPB, lateral/medial parabrachial nucleus; RRF, retrorubral field; Sol, nucleus of the solitary tract; PCRt, parvocellular reticular formation.

(C) Optical depolarization of ChR2-expressing VGat-*Cre* CeA neurons in slices. 0.5s-long 473-nm light at 1 Hz and 10 ms at 1, 5, 10, and 20 Hz.

(D) CeA optogenetic stimulation is performed concomitantly to dual-electromyogram recordings from the jaw-closing masseter and the head-orienting trapezius muscles (blue and red traces, respectively).

(E) Representative optogenetically evoked electromyogram traces from two mice. Shaded blue area represents laser ON periods.

(F) Average onset and offset values associated with enhanced electromyogram signals upon laser activation (n = 5, two-way repeated-measures (RM) ANOVA muscle effect p = 0.88).

(G) CeA optical activation reduced the time needed for mice to successfully capture cricket prey of different sizes (n = 5, two-way RM ANOVA main effect of laser $F[1,4] = 24.0$, $^*p = 0.008$).

(H) CeA optical activation increased number of bites on body parts other than the prey's head (n = 5, $F[1,4] = 41.4$, $^*p = 0.003$).

(I) Left: latency to initiate pursuit of prey was unaffected by laser in either internal state (n = 5, $F[1,4] = 5.4$, $p = 0.08$). Right: however, subtracting oromotor segments reveals reduced latencies in sated mice (n = 5, laser × hunger $F[1,4] = 231.2$, $^*p < 0.001$).

(J) CeA optical activation elicited predatory-like attacks on a moving artificial insect (%time attacking prey, n = 5, $F[1,4] = 8.5$, $^*p = 0.04$). See also Movie S2.

(K) Two-dimensional masseter × trapezius space populated with *Z* scores from electromyogram traces. Unsupervised cluster analysis failed to discriminate between laser off trials and no hunting events. In contrast, both optical activation and natural hunting were associated with clusters located in the upper-right quadrant, indicating strong masseter-trapezius co-activation. Black crosses represent the clusters' centroids and green dots represent misclassifications.

(L) CeA optical activation elicited the seizing, biting, and eventual ingestion of non-food objects, particularly strongly in hungry mice (n = 5, laser effect, $F[2,8] = 179.2$, $^*p < 0.001$, laser × hunger $F[2,8] = 224.7$, $p < 0.001$). See also Movie S3. BL, baseline laser off.

(M–P) Chemogenetic activation of CeA elicited increased number of bites outside the prey's head (n = 5, CNO effect $t[4] = 5.35$, $^*p = 0.006$, M); faster pursuit (n = 5, $t[4] = 3.6$, $^*p = 0.02$, N), shorter latencies to pursuit (n = 5, $t[4] = 4.6$, $^*p = 0.009$, O) and more efficient hunting (n = 5, $t[4] = 3.7$, $^*p = 0.02$, (P).

(Q) Chemogenetic activation of CeA elicited predatory-like attacks on a moving artificial insect, n = 5, $t[4] = 5.7$, $^*p = 0.005$,. See also Movie S2.

(R–T) Chemogenetic inhibition of CeA caused slower pursuit (n = 5, $t[4] = 2.8$, $^*p = 0.04$, R), increased latencies (n = 5, $t[4] = 4.2$, $^*p = 0.01$, S), and less efficient hunting (n = 5, $t[4] = 2.7$, $^*p = 0.04$, T). CNO, clozapine-N-oxide designer activator.

Data are reported as mean ± SEM. See also Figure S1 and Movies S1, S2, and S3.

et al., 1980; Nikulina, 1981) optogenetic activation of CeA shortened the time needed for mice to capture and subdue their prey (Figures 1G–1I, S1H, and S1I). Captured crickets were immediately eaten.

Optogenetic activation of CeA led mice to pursue, bite, and restrain moving artificial prey independently of internal state (Figures 1J and S1J; Movie S2). Such attacks were never observed when laser source was off. Stretching of the neck and the release of biting attacks, concomitant to "prey" restraint using the forepaws, characterized these responses to optical stimulation (Movie S2). CeA optical activation thus mimicked the prototypical posture observed during insect hunting (Finlay et al., 1980).

Enhanced predatory efficiency upon CeA stimulation was mirrored by analyses of electromyogram recordings. *Z* scores from the electromyogram traces recorded during both natural hunting and CeA optical stimulation alone were plotted onto the two-dimensional masseter × trapezius space (Figure 1K). Unsupervised clustering algorithms assigned both optical activation and natural hunting to clusters located in the upper-right quadrant due to masseter-trapezius co-activation. Interestingly, these two clusters were separated, with optical activation producing more robust muscle activation than natural hunting.

Generally, upon laser activation, mice readily seize, bite, and often ingest, non-edible objects, an effect that was modulated by internal state (Figure 1L; Movie S3). Laser activation also abolished natural preferences for edible over non-edible items (Figures S1K–S1P). Optically stimulating the CeA of VGat-ires-*Cre* mice injected with the non-excitable *Cre*-inducible control construct AAV-EF1a-DIO-EYFP revealed no effects on any of the hunting parameters measured (Figures S1Q–S1S). Moreover, ChR2 transfection and optical stimulation of the neighboring striatal and *globus pallidus* areas of VGat-ires-*Cre* mice also failed to elicit any effects on hunting (Figures S1T–S1Y). Finally, consummatory acts toward non-edible items were specifically and completely abolished upon interrupting GABA release from CeA terminals (Figures S1Z–S1DD).

Chemogenetic approaches (Sternson and Roth, 2014) corroborated the optogenetic studies. The *Cre*-inducible excitatory designer receptor encoded in the construct AAV-hSyn-HA-hM3D(Gq)-IRES-mCherry was injected into the CeA of VGat-ires-*Cre* mice. Administering the designer drug clozapine-N-oxide (CNO) increased both lethal bites unrestricted to the insects' head (Figure 1M) and pursuit velocities (Figure 1N). Latencies to pursuit were shortened (Figure 1O), as were capture durations (Figure 1P). CNO administration also produced attacks on artificial prey (Figure 1Q; Movie S2). We also injected the CeA of VGat-ires-*Cre* mice with the *Cre*-inducible inhibitory designer receptor encoded in the construct AAV-hSyn-HA-hM4D(Gi)-IRES-mCherry. Consistently, in these mice CNO administration led to a striking decrease in hunting efficiency (Figures 1R–1T).

Central Amygdala Activation Did Not Induce Attacks on Conspecifics, Greater Food Intake, or Anxiety-like Behaviors

We failed to observe any occurrences of attacks on conspecifics upon CeA activation (Figure S1EE), ruling out nonspecific aggression. Also, laser activation did not increase total ingestion of either of two types of food pellets presented (Figure S1FF), ruling out laser-induced physiological need. Consistently, both chemogenetic activation and inhibition of CeA failed to alter food intake (Figures S1GG–S1HH). Finally, open-field tests failed to reveal any anxiogenic patterns potentially induced by either activation or inhibition of CeA (Figures S1II–S1PP).

Changes in Central Amygdala Neuronal Activity Preceded Prey Capturing

In order to evaluate the behavior of CeA neuronal populations during active hunting, we performed electromyogram monitoring of the masseter muscle concomitantly to array neuronal recordings. Principal component analyses of the neuronal data revealed that ~40% of the recorded neurons increased activity during insect hunting (Figures 2A and S2), with hunting-excited CeA neurons maintaining activity levels throughout prey pursuit (Figure 2C).

The delivery of bites aimed at prey was accompanied by a sharp, transient increase in masseter activity. Principal component analyses revealed that this was concomitant to the emergence of capture-excited neurons in CeA (~36%, Figures 2D–2F). Finer temporal scale analyses confirmed that capture-excited neurons tended to increase activity just prior to the attempt to capture (Figures 2G and 2H). These patterns are consistent with the perspective that CeA commands prey capture, in agreement with the effects of optical stimulation. Finally, a significant proportion of CeA neurons increased their activity levels during the consumption of prey (~40%, Figure 2I).

The Central Nucleus of the Amygdala Controls Cervical-Mandibular Systems by Acting on Inhibitory Interneurons of the Parvocellular Reticular Formation

CeA transfection in VGat-ires-Cre mice with the ChR2 construct modified to encode a fluorophore fused to synaptobrevin (AAV-EF1a-DIO-Synb-eGFP, Land et al., 2014) revealed a dense CeA terminal field in the brainstem reticular formation (Shammah-Lagnado et al., 1992; Van Daele et al., 2011). Expression was densest throughout rostral-to-caudal levels of the parvocellular reticular formation (PCRt, Figures 3A–3C). PCRt is known to contain a large population of both inhibitory (VGat expressing) and excitatory (VGlut2 expressing) craniofacial premotor neurons (Stanek et al., 2014; Travers and Norgren, 1983). Accordingly, *Cre*-dependent transfection of both VGat and VGlut2 neurons in PCRt with the retrograde pseudotyped rabies virus SADΔG-GFP(EnvA) (Wickersham et al., 2007) resulted in neuronal labeling in the medial part of CeA (Figures 3D and 3E; for lower magnification, see Figure S3A). Locations of rabies-labeled cells throughout CeA levels are shown in Figure S3P.

To assess the functional relevance of the CeA → PCRt projections, *VGat-ires-Cre mice* were transfected with *Cre*-dependent ChR2 in CeA and optical fibers placed immediately above the CeA neuronal terminals in PCRt. When animals were placed on empty cages, stimulation of CeA → PCRt projections induced "fictive feeding" behaviors, i.e., mice faithfully executed feeding-like sequences (Farr and Whishaw, 2002) in the absence of food. Specifically, upon laser activation, mice immediately interrupted locomotion (Figures S3B–S3E), sit back on their haunches, brought elbows inward periodically as if holding food with the forepaws, and displayed rhythmic oral movements (Figure 3F; Movie S4). Fictive feeding was elicited independently of internal state (Figure 3F). Additionally, whereas CeA → PCRt activation led to sustained mastication of non-food items, it failed to increase overall food intake (Figures S3F–S3I).

According to the above-mentioned rabies-based retrograde patterns, CeA neurons directly contact inhibitory VGat neurons in PCRt. We thus reasoned that CeA → PCRt activation might release feeding programs from inhibition. We specifically hypothesized that stimulating VGat neurons in PCRt would be sufficient to disrupt the ability of CeA → PCRt activation to release feeding programs. We employed a combination of optogenetics and chemogenetics (Sternson and Roth, 2014) to test this

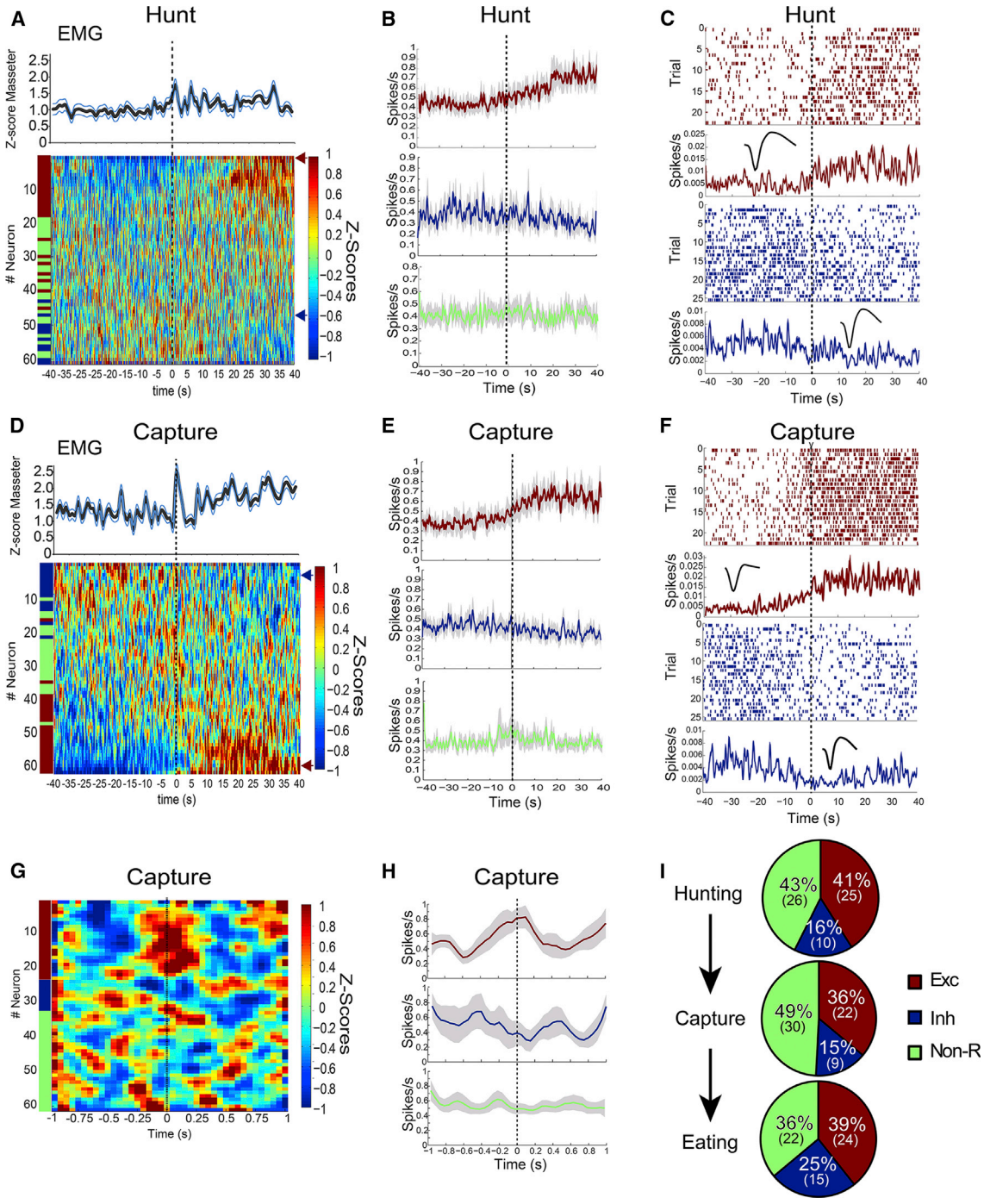

Figure 2. Neuronal Dynamics in Central Amygdala during Prey Capturing

During active hunting, electromyogram monitoring of the masseter muscle was performed concomitantly to array neuronal recordings from CeA.

(A) Concurrently to enhanced masseter activity, approximately 40% of the recorded neurons displayed increased activity during insect hunting. T = 0 denotes the time when insect pursuit starts. The heatmap displays the first principal component associated with the *Z* scores of each neuron recorded during these sessions, ranked according to the *Z* score values (i.e., the neuron displaying the greatest increases in activity is shown on top, through the neuron displaying the greatest drop in activity, shown at bottom). *Z* scores were computed as deviations from the overall mean firing rate throughout the hunting sessions. Neurons were deemed excited or inhibited by hunting based on event-related statistical analyses of the *Z* scores. As shown in the lower part of the heatmap, ~16% of the neurons were inhibited during hunting.

(B) Computing the mean population activity from the subset of neurons deemed excited (red) or inhibited (blue) by hunting revealed that altered activity persisted throughout prey pursuit. Green trace shows the mean population activity extracted from the subset of neurons deemed unaffected by hunting.

(legend continued on next page)

hypothesis. VGat-ires-Cre mice were ChR2-tranfected in CeA and optical fibers placed in PCRt as above. To reversibly increase inhibitory tone within PCRt, the same animals were injected into PCRt with the *Cre*-dependent designer receptor (Figures 3G and 3H). We found that administering CNO completely suppressed masseter and trapezius electromyogram responses to optical stimulation (Figures 3I and 3J and S3J–S3M). Efficacy of the chemogenetic approach was confirmed in vivo (Figures S3N and S3O).

To further assess the specificity of the VGat(CeA) → VGat(PCRt) projection in releasing feeding programs, we introduced the viral construct AAV-flex-taCasp3-TEVp (Yang et al., 2013), which induces *Cre*-dependent caspase expression, into the PCRt of both VGat-ires-*Cre* and VGlut2-ires-*Cre* mice (Figures 3K and 3L). The CeA of these same animals were concomitantly transfected with non-*Cre*-dependent AAV-ChR2. Only caspase-treated VGat-ires-*Cre* animals failed to display cervical-mandibular activity in response to optical activation of CeA, as shown by electromyogram analyses (Figures 3M and 3N). In sum, CeA releases craniofacial activity via disinhibition of the parvocellular reticular circuitry.

The Parvocellular Reticular Formation Contains Both Mandibular and Cervical Premotor Neurons

We investigated in greater depth the reticular circuitry mediating CeA control over craniofacial musculatures. The rabies construct SADΔG-GFP(EnvA) was injected into either the jaw-controlling motor trigeminal nucleus ("Mo5"), or the neck-controlling accessory motor nucleus ("11N") of *ChAT-ires-Cre* × RΦGT mice (Figures S4A–S4H). Only PCRt—and to a lesser extent the immediately adjacent intermediate reticular nucleus—was found to contain premotor neurons to both Mo5 and 11N (Figure S4I). Moreover, VGat neurons in PCRt directly targeted these motor nuclei (Figures S4J–S4M).

Inhibitory Interneurons in PCRt Bi-directionally Control Mandibular and Cervical Musculatures

We used optogenetics to probe the function of excitatory and inhibitory PCRt populations (Figures 4A and 4B and S4N–S4R). In hungry mice offered food pellets, activation of PCRt *VGat*-positive neurons produced a rapid arrest in oromotor activity, which was immediately resumed upon laser deactivation (Figure 4C; Movie S4). Consistently, this optical stimulation caused an immediate suppression of electromyographic activity in both masseter and trapezius (Figures 4D, 4E, and S4S).

Intriguingly, optical stimulation of PCRt *VGlut2* neurons caused only minor effects in electromyography traces (Figures 4F and S4T). In contrast, optical inhibition of *VGat*-positive neurons in PCRt using the hyperpolarizing green-light-sensitive channel archeorhodopsin (Madisen et al., 2012) significantly stimulated electromyographic activity in both masseter and trapezius (Figures 4G, S4U, and S4V). This effect was accompanied by evident oromotor behaviors.

Inhibitory Neurons in PCRt Mediate the Delivery of Killing Bites but Not Prey Pursuit

Based on the above, we reasoned that both optical and tonic depolarization of PCRt VGat neurons should attenuate the potential for mice to successfully hunt insect prey. Activating designer receptors specifically in PCRt *VGat* neurons completely suppressed the ability to kill and consume crickets (Figure 4H). CNO-treated mice incapacitated mice to deliver killing bites despite the fact that prey were intensively pursued and kept subdued with the assistance of the forepaws (Figures 4I and 4J; Movie S5). This led to numerous pursuit events upon CNO treatment (Figure 4K). Similar effects were observed using optogenetic activation of PCRt *VGat* neurons (Movie S5). In fact, *VGat* neuron activation impaired mastication while preserving the ability to reach for pellets in a forepaw-based pellet-reaching task (Figures S4W–S4Z).

Central Amygdala Projections to the Periaqueductal Gray Matter Control Prey Pursuit

The periaqueductal gray matter (PAG) is a major CeA target previously implicated in predatory attacks (Comoli et al., 2005; Shaikh et al., 1985). We thus hypothesized a role for CeA → PAG projections in predatory hunting. Synaptobrevin expression analyses revealed a continuous terminal field throughout the ventrolateral and lateral aspects of PAG (VLPAG and LPAG, Figure 5A). Consistently, slice electrophysiological mapping studies confirmed that optogenetic activation of CeA *VGat*-terminals robustly inhibited their PAG neuronal targets (Figures S5A–S5C). Likewise PCRt, *Cre*-dependent SADΔG-GFP(EnvA) rabies transfection of both $VGat^{+}$ and $VGlut2^{+}$ PAG neurons resulted in neuronal labeling in CeA (Figures 5B, 5C, and S5D–S5E). Locations of rabies-labeled cells throughout CeA levels are shown in Figure S3P.

To assess the functional relevance of these CeA → PAG projections, VGat-ires-*Cre* mice were transfected with non-*Cre*-dependent ChR2 in CeA and optical fibers placed immediately above the CeA neuronal terminals in LPAG/VLPAG. In the same animals, the *Cre*-inducible excitatory chemogenetic construct AAV-hSyn-HA-hM3D(Gq)-IRES-mCherry was injected into the PAG of both VGat-ires-*Cre* and VGlut2-ires-*Cre* mice (Figures S5F and S5G). CeA → PAG optical activation enhanced

(C) Analyses of individual raster plots revealed that hunting-excited (red raster) and hunting-inhibited (blue raster) maintained altered activity levels throughout prey pursuit. Representative cases are shown. Note corresponding waveform in insert.
(D–F) Similar analyses as in (A)–(C), but this time attempts to capture a prey were defined as the event of interest. Note that the delivery of bites aimed at prey was accompanied by a sharp, transient increase in masseter electromyographic activity. Changes in neuronal activity during prey capture T = 0 denotes the moment when capture is attempted (D). Mean population activity around prey capture (E). Individual raster plots associated with prey capture events (F).
(G) Analyses of neuronal activity based on a finer temporal scale revealed that, overall, capture-excited neurons tended to increase activity just previous to the attempt to seize prey with jaws and forepaws. A similar, symmetrical effect was associated with CeA neurons whose activity declined immediately previous to the attempt to capture.
(H) First Principal Component extracted from the subset of neurons deemed excited (red), inhibited (blue), or unaffected (green) by attempt to capture prey.
(I) Relative proportions of neurons deemed excited (red), inhibited (blue), or unaffected (green) by hunting/capturing/eating prey.
Data are reported as mean ± SEM. See also Figure S2.

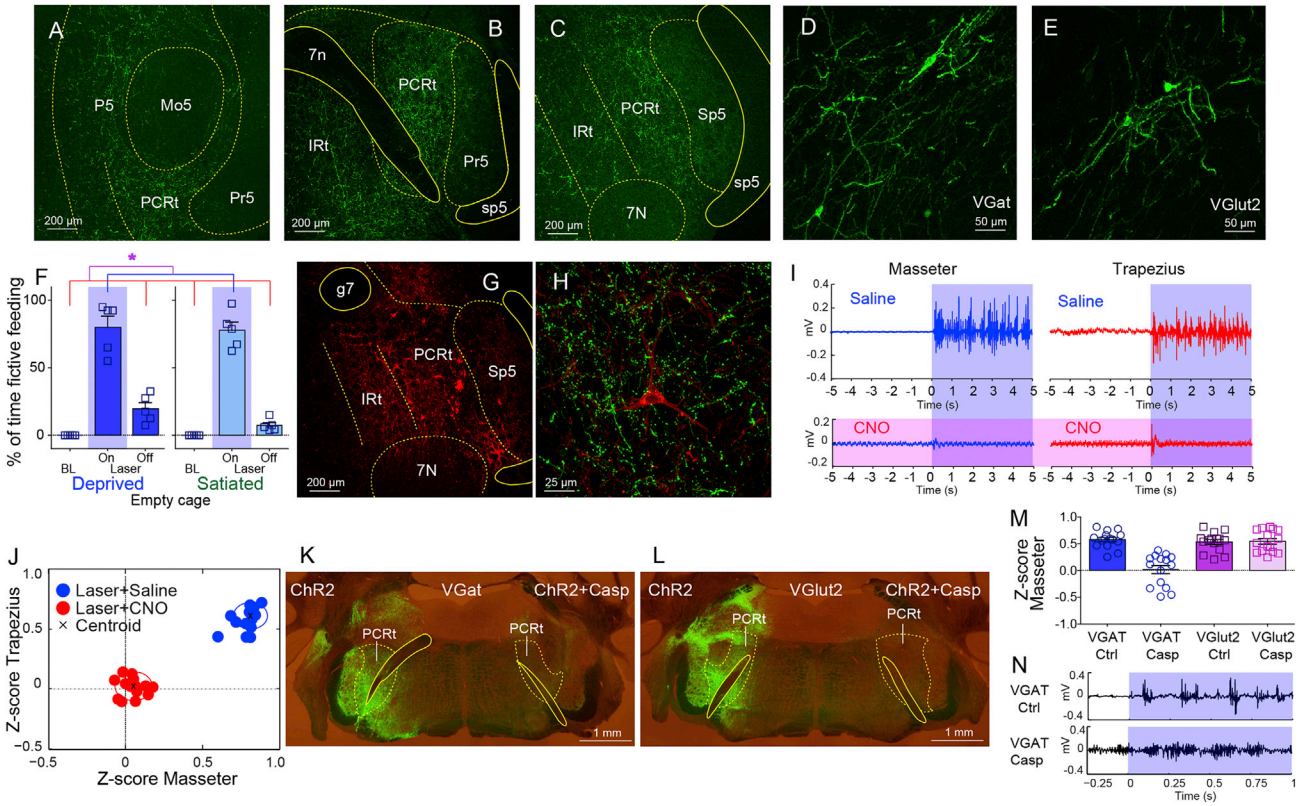

Figure 3. Central Amygdala Controls Cervical-Mandibular Systems by Acting on Inhibitory Interneurons of the Parvocellular Reticular Formation

(A–C) *Cre*-dependent synaptobrevin-fused eGFP transfection was induced in CeA of VGat-ires-*Cre* mice. GFP-labeled punctate patterns imply putative synapses. Coronal sections reveal dense terminal fields in PCRt, from rostral regions adjacent to Mo5 through more caudal regions adjacent to 7N (A) through (C). No expression was observed within motor nuclei. 7N, motor nucleus VII; 7n, facial nerve tract; IRt, intermediate reticular formation; Mo5, motor nucleus V; P5, peritrigeminal zone; Pr5, principal sensory trigeminal nucleus; Sp5, spinal trigeminal nucleus; sp5, spinal trigeminal tract.

(D) *Cre*-dependent pseudotyped rabies virus SADΔG-GFP(EnvA) was injected in PCRt of VGat-ires-Cre mice. The panel shows several retrogradely labeled neurons in centromedial amygdala (CeM), revealing direct CeM → PCRt(VGat) contacts.

(E) Same as (D) but for VGut2-ires-*Cre* mice.

(F) Frequency of laser-induced fictive feeding, which was elicited in both hungry and sated states (n = 5, two-way RM ANOVA main effect of laser $F[2,8] = 196.8$, $^*p < 0.001$).

(G) Coronal section shows *Cre*-dependent designer receptor-fused mCherry expression in PCRt of VGat-ires-Cre mice. g7, *genus* of facial nerve.

(H) In the same mouse, CeA was transfected with synaptobrevin and with the designer receptor in PCRt. Panel shows a VGat neuron in PCRt (tagged by mCherry) targeted by CeA synapses (tagged by eGFP).

(I) VGat-ires-Cre mice were transfected with the *Cre*-dependent depolarizing designer receptor in PCRt and ChR2 in CeA. Panel shows electromyogram activity of masseter (left, blue) and trapezius (right, red) evoked by optical stimulation of CeA → PCRt projections. Shown are representative electromyogram traces; shaded blue area represents laser on period. The lower panels (in purple) reveal that administering the designer drug CNO completely abolished the ability of CeA to synergize the masseter and trapezius muscles.

(J) *Z* scores from electromyogram patterns were plotted on the two-dimensional masseter × trapezius space. In all cases laser was on. Cluster separation of trials in which saline (blue cluster) versus CNO (red cluster) were administered. Note abolished muscle synergy in CNO trials. Black crosses represent the clusters' centroids.

(K and L) A different cohort was unilaterally transfected with *Cre*-inducible ChR2 (left hemisphere) and ChR2+Caspase (right) in PCRt of VGat-ires-*Cre* (K) and VGlut2-ires-*Cre* (L) mice. The panels illustrate efficacy of caspase treatment.

(M) *Z* scores associated with the differential electromyogram signal from masseter induced by optical CeA activation in VGat-ires-*Cre* and VGlut2-ires-*Cre* mice treated with *Cre*-dependent caspase in PCRt. Only ablation of VGat neurons in PCRt abolished the ability of CeA to recruit masseter activity. Each dot represents a separate "laser ON" trial (n = 45, $F[3,56] = 23.08$, $^*p < 0.001$).

(N) The above effect observed in caspase-treated mice was due to high baseline masseter activity caused by inhibitory neuronal ablation. This then blunted *Z* scores associated with laser-induced activation. Representative masseter traces from control (upper panel) and ablated (lower) mice are shown. Note higher baseline level in ablated mouse.

Data are reported as mean ± SEM. See also Figure S3 and Movie S4.

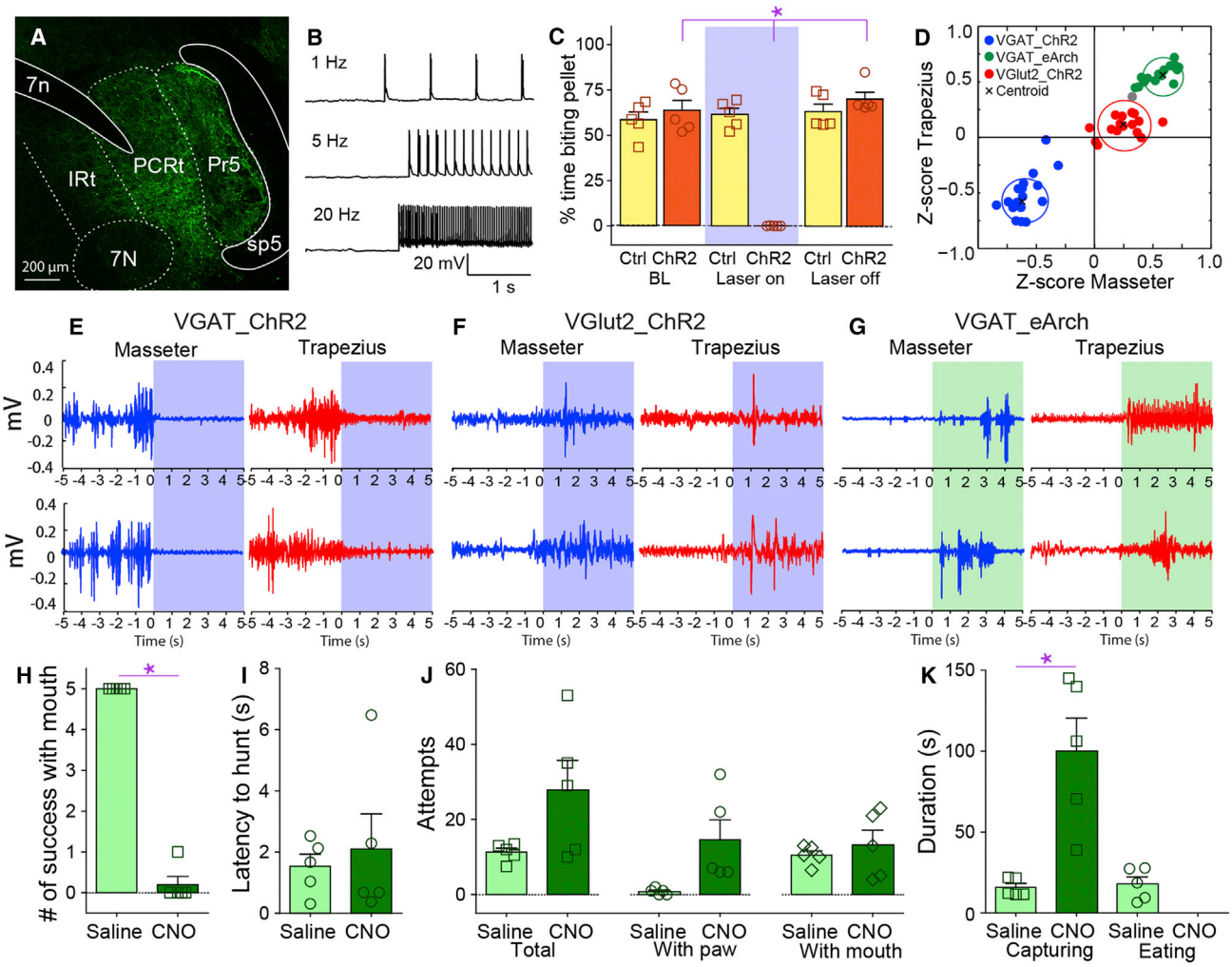

Figure 4. Inhibitory Interneurons of the Parvocellular Reticular Formation Bi-directionally Control Mandibular and Cervical Musculatures

(A) Coronal section illustrating *Cre*-dependent ChR2 expression in PCRt of VGat-ires-Cre mice. Optical fibers were stereotaxically placed into PCRt. 7N, (Facial) motor nucleus VII; 7n, facial nerve tract; IRt, intermediate reticular formation; Mo5, (Trigeminal) motor nucleus V; PCRt, parvocellular reticular formation; Pr5, principal sensory trigeminal nucleus; sp5, spinal trigeminal tract.

(B) Representative traces showing optogenetic activation of ChR2-expressing VGat neurons in PCRt by blue laser at 1, 5, and 20 Hz.

(C) Optical activation of PCRt VGat neurons immediately and reversibly abolished eating in hungry mice (%time biting pellet, two-way RM ANOVA main effect of laser n = 5, $F(2,8) = 47.7$, *$p < 0.001$). Note that laser produces no effect whatsoever on control mice (Ctrl) transfected with *Cre*-dependent EYFP unresponsive to light.

(D) *Z* scores from electromyogram patterns were plotted on the two-dimensional masseter × trapezius space. Unsupervised cluster analysis fully discriminated trials in which blue laser activated ChR2 in VGat neurons (blue cluster), versus trials in which green laser activated eArch in VGat neurons (green cluster), versus trials in which blue laser activated ChR2 in VGlut2 neurons (red cluster). Black crosses represent the clusters' centroids. Note strong inhibition (lower-left quadrant) and excitation (upper- right quadrant) of masseter and trapezius produced by ChR2 and eArch activation in VGat-ires-Cre mice, respectively. Note also weak effects produced by PCRt VGlut2-neuron depolarization on muscle activity (center of graph).

(E–G) Illustrative electromyogram traces (masseter in blue, trapezius in red) are shown for each case. Blue and green shaded areas show periods when blue and green lasers were on, respectively. During eating, cranio-cervical muscle activity was abolished upon optical activation of PCRt VGat-neurons (E). Effects of optical activation of PCRt VGlut2-neurons on cranio-cervical muscle contractions (F). Cranio-cervical muscle activity was stimulated upon optical inhibition of PCRt VGat-neurons (G).

(H) VGat-ires-Cre mice were transfected with the *Cre*-dependent depolarizing designer receptor in PCRt. Administering the designer drug CNO completely abolished the ability to capture insects using the jaws (n = 5, paired t test $t[4] = 24.0$, *$p < 0.001$).

(I) CNO administration did not affect latency to hunt, as mice actively pursued crickets despite oromotor impairments (n = 5, $t[4] = 0.4$, $p = 0.7$).

(J) CNO administration did not produce major effects on total number of capture attempts (all $p > 0.05$).

(K) However, CNO administration significantly lengthened the time interval required to successfully capture crickets, with capturing requiring forepaws use after CNO injections (n = 5, $t[4] = 4.1$, *$p = 0.01$).

Data are reported as mean ± SEM. See also Figure S4 and Movie S5.

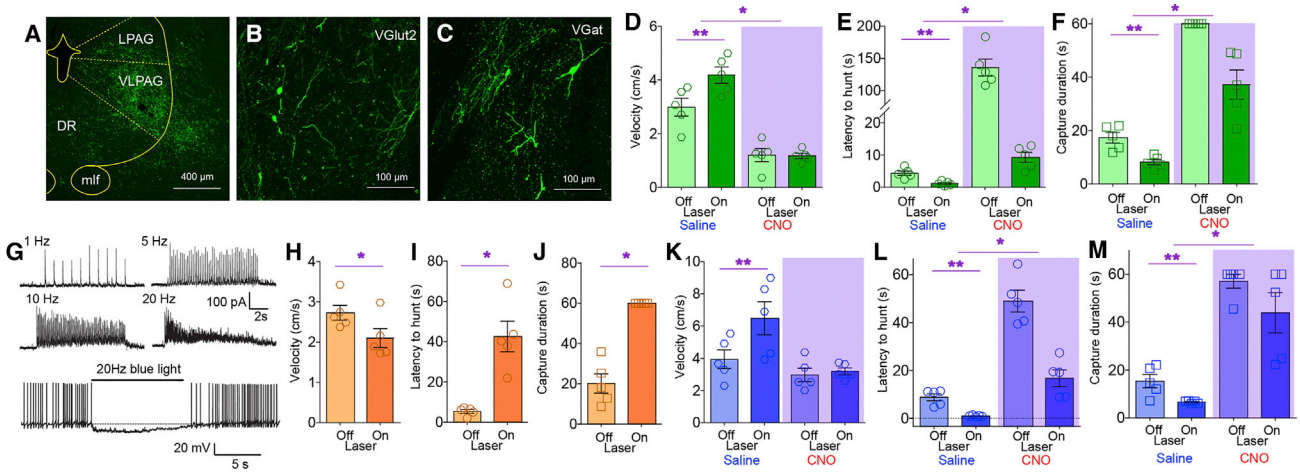

Figure 5. Central Amygdala Projections to the Periaqueductal Gray Matter Control Prey Pursuit

(A) *Cre*-dependent synaptobrevin-fused eGFP was virally transfected in CeA of VGat-ires-*Cre* mice. GFP-labeled punctate patterns imply putative synapses. Coronal sections reveal dense terminal fields in ventrolateral/lateral (VL/L) PAG, extending ventrolaterally into the mesencephalic reticular formation. DR, dorsal raphe; mlf, medial longitudinal fasciculus.

(B) *Cre*-dependent pseudotyped rabies virus SADΔG-GFP(EnvA) was injected in VL/L PAG of VGlut2-ires-*Cre* mice. The panel shows retrogradely labeled neurons in centromedial amygdala (CeM), revealing direct CeM → PAG[VGlut2] contacts.

(C) Same as (B) but for VGgat-ires-*Cre* mice.

(D–F) Optical activation of CeA → PAG projections elicited moderately faster prey pursuit (n = 5, paired t test **p = 0.03, D), much shorter latencies to pursuit (**p = 0.006, E), and more efficient hunting (**p = 0.02, F). However, all these effects were totally annulled by chemogenetic activation of VGlut2 neurons in PAG (for D–F, two-way RM ANOVA CNO effect F[1,4] > 90.0, *p < 0.002).

(G) (four upper panels) Representative traces of hyperpolarizing currents recorded fromVGlut2 neurons in PAG under current-clamp mode. The traces show the effects of optically stimulating CeA fibers terminating onto these neurons with blue laser at 1, 5, 10, and 20 Hz. (lower panel) Voltage-clamp recordings showing that photostimulation of CeA-ChR2 terminals (20 Hz) in PAG hyperpolarized and inhibited PAG VGlut2 neurons.

(H–J) Optical activation of PAG[VGlut2] → MLR projections elicited slower prey pursuits (n = 5, paired t test *p = 0.009, H), much longer latencies to pursuit (*p = 0.006, I), and less efficient hunting (*p = 0.001, J).

(K–M) On a different cohort of mice, optical activation of CeA → PAG projections once again elicited faster prey pursuit (n = 5, paired t test **p = 0.01, K), much shorter latencies to pursuit (**p = 0.01, L), and more efficient hunting (**p = 0.03, M). However, the enhancing effects of laser stimulation on latencies to pursuit and hunt efficiency were annulled by chemogenetic activation of MLR neurons (for L–M, n = 5, two-way RM ANOVA CNO effect F[1,4] > 60.0, *p < 0.002; for K, F[1,4] = 6.3, p = 0.06).

Data are reported as mean ± SEM. See also Figure S5 and Movie S6.

predatory hunting (Movie S6). Specifically, CeA → PAG optical activation increased pursuit velocities (Figure 5D) and shortened both latency to pursue and overall hunting duration (Figures 5E and 5F).

To counter the inhibitory effects of CeA on PAG neurons, we combined optical stimulation with administration of the designer drug CNO in both VGlut2-ires-*Cre* and VGat-ires-*Cre* mice. We found that all of the hunting-promoting effects produced by optical stimulation were annulled by CNO injections in VGlut2-ires-*Cre* mice (Figures 5D–5F). This is consistent with CeA terminals inhibiting their VGlut2-expressing target cells in PAG (Figure 5G). CNO treatment in VGat-ires-*Cre* mice failed to significantly alter optically induced hunting (Figures S5H–S5J). Finally, and in contrast to CeA → PCRt, CeA → PAG activation failed to induce either fictive feeding or approach toward non-food items (Figures S5K–S5O).

Periaqueductal Gray Matter Projections to the Mesencephalic Locomotor Region Gate Predatory Hunting

We investigated in greater depth the downstream targets of the hunting-controlling PAG[VGlut2$^+$] neurons. Interestingly, analyses of *Cre*-inducible synaptobrevin expression revealed that VGlut2 neurons in VLPAG/LPAG project densely to dorsolateral midbrain (e.g., pendunculopontine and cuneiform nuclei Figure S5Q). These areas are located within the mesencephalic locomotor region ("MLR," Skinner and Garcia-Rill, 1984). In contrast, similar synaptobrevin analyses failed to reveal terminals in MLR of VGat-ires-*Cre* mice (Figure S5R). The functionality of the PAG[VGlut2$^+$] → MLR pathway was further suggested by combining *Cre*-inducible synaptobrevin and retrograde labeling (Figure S5S). We then transfected VLPAG/LPAG of VGlut2-ires-*Cre* mice with *Cre*-dependent ChR2, and optical fibers were placed immediately above the PAG neuronal terminals in MLR. As expected, optical activation caused a significant reduction in pursuit velocity (Figure 5H), as well as significant increases in both latency to pursue (Figure 5I) and prey capture duration (Figure 5J).

Central Amygdala Controls the Mesencephalic Locomotor Region via the Periaqueductal Gray Matter

Finally, we tested the presumed functionality of the CeA → PAG → MLR pathway. In the same VGat-ires-*Cre* mice, we transfected the CeA with *Cre*-inducible ChR2, implanted optical fibers

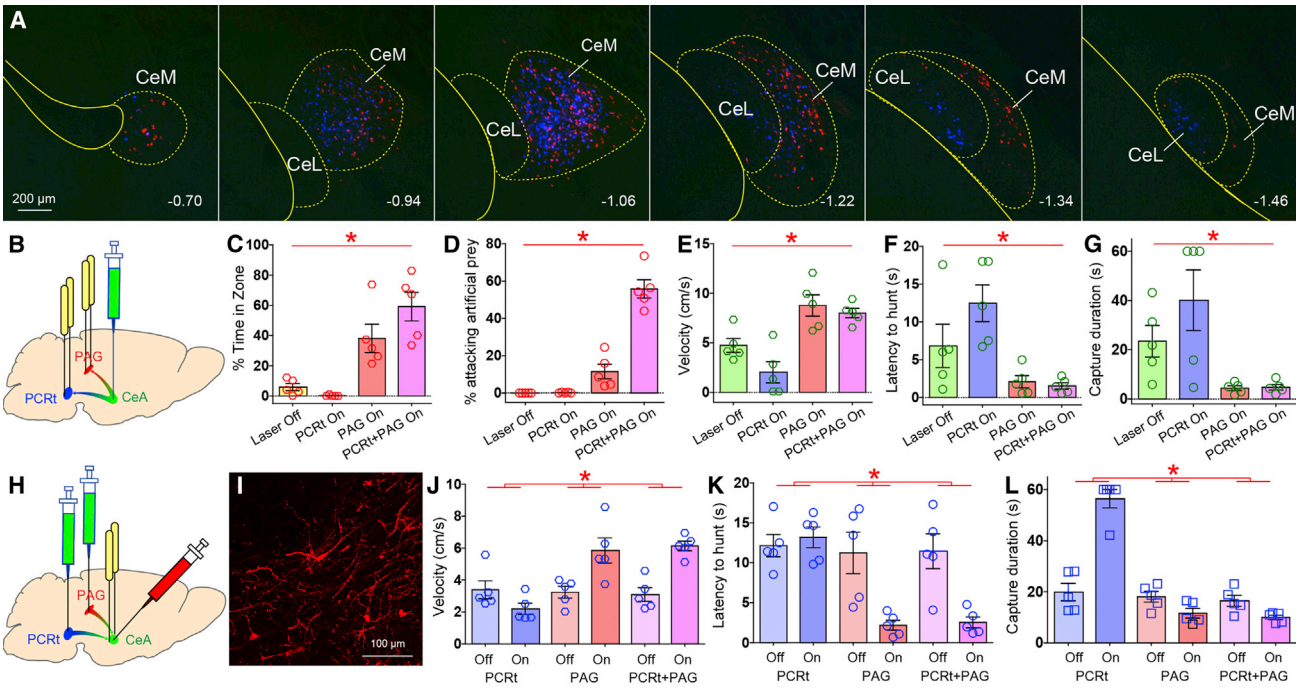

Figure 6. Co-activation of Central Amygdala Terminals in the Reticular Formation and Central Gray Is Sufficient to Induce Predatory Behavior

(A) In the same animals, FluoroGold injections in PCRt and CTb injections in VL/LPAG resulted in labeling of neurons throughout CeA. Merging reveals that primarily separate CeA populations project to these two descending centromedial amygdala (CeM) targets. While both subpopulations densely label the centromedial amygdala (CeA), at more caudal levels in centrolateral amygdala (CeL) they appear as spatially segregated. The numbers below indicate distance from bregma. Neighboring striatum and *glubus pallidus* were not retrogradely labeled.

(B) In the same group of VGat-ires-*Cre* mice, CeA was transfected with *Cre*-inducible ChR2, and optical fibers implanted bilaterally onto CeA terminals in both PAG and PCRt.

(C) Activating the CeA → PAG pathway alone was sufficient to cause pursuit of artificial prey, as shown by the time spent in the vicinity of the robot prey (n = 5, two-way RM ANOVA laser effect $F[1,4] = 42.8$, $p^* = 0.003$).

(D) However, only the combined CeA → PAG+CeA → PCRt stimulation gave rise to sustained biting attacks upon escaping artificial prey (laser effect $F[1,4] = 86.4$, $p^* = 0.001$; CeA → PAG+CeA → PCRt versus other conditions, paired t test Bonferroni all $p < 0.03$).

(E–G) During hunting of live prey, optical activation of both CeA → PAG alone and CeA → PAG+CeA → PCRt elicited faster prey pursuits (n = 5, laser effect $F[1,4] = 21.6$, $p^* = 0.001$, E), shorter latencies to pursuit ($F[1,4] = 5.0$, $p^* = 0.008$, F), and more efficient hunting $F[1,4] = 51.4$, $p^* = 0.002$, G). Generally, activating CeA → PCRt alone produced detrimental effects on hunting.

(H) Three different groups of wild-type mice were transfected with the retrograde CAV2-*Cre*-GFP construct into PCRt and/or PAG. CeA was then transfected with *Cre*-inducible ChR2-mCherry and implanted with optical fibers.

(I) *Cre*-inducible expression of ChR2-mCherry in CeA of a mouse injected with CAV2-GFP-*Cre* in PCRt and PAG.

(J–L) During hunting of live prey, optical activation of both CeA → PAG alone and CeA → PAG+PCRt elicited faster prey pursuits (n = 5 per group, laser × group effect $F[2,12] = 11.2$, $p^* = 0.002$, J), shorter latencies to pursuit ($F[2,12] = 83.5$, $p^* = 0.01$, K), and more efficient hunting $F[2,12] = 70.1$, $p^* < 0.001$, L). Again, activating CeA → PCRt alone produced detrimental effects on hunting.

Data are reported as mean ± SEM. See also Figure S6 and Movie S2.

above CeA terminals in PAG, and transfected the MLR with the non-*Cre*-dependent excitatory chemogenetic designer receptor. We hypothesized that administering the designer drug CNO would negate the hunting promoting effects produced by CeA → PAG optical activation. In other words, we predicted that this treatment would mimic the effects of activating PAG VGlut2 neurons during prey pursuit. Consistently, CNO administration completely annulled the hunt-promoting effects of CeA → PAG activation on pursuit latencies and capture duration, albeit having a more modest suppressing effect on velocities (Figures 5K–5M). Importantly, all experiments involving the PAG → MLR pathway failed to influence performance on open-field tests (Figures S5T–S5W).

Co-activation of the CeA → PCRt and CeA → PAG Pathways Is Sufficient to Induce Robust Hunting

From the series of studies above, we inferred that different CeA downstream targets mediate craniofacial control versus prey pursuit. Consistently, dual retrograde tracer injections in PAG and PCRt revealed that CeA neuronal groups projecting to PAG versus PCRt are largely segregated (Figure 6A). We then analyzed the effects of activating both pathways simultaneously.

In the same VGat-ires-*Cre* mice, we transfected the CeA with *Cre*-inducible ChR2 and implanted bilateral optical fibers above CeA terminals in both PAG and PCRt (Figures 6B and S6A). Although activating the CeA → PAG pathway alone led mice to pursue artificial prey, only stimulation of the CeA → PAG +

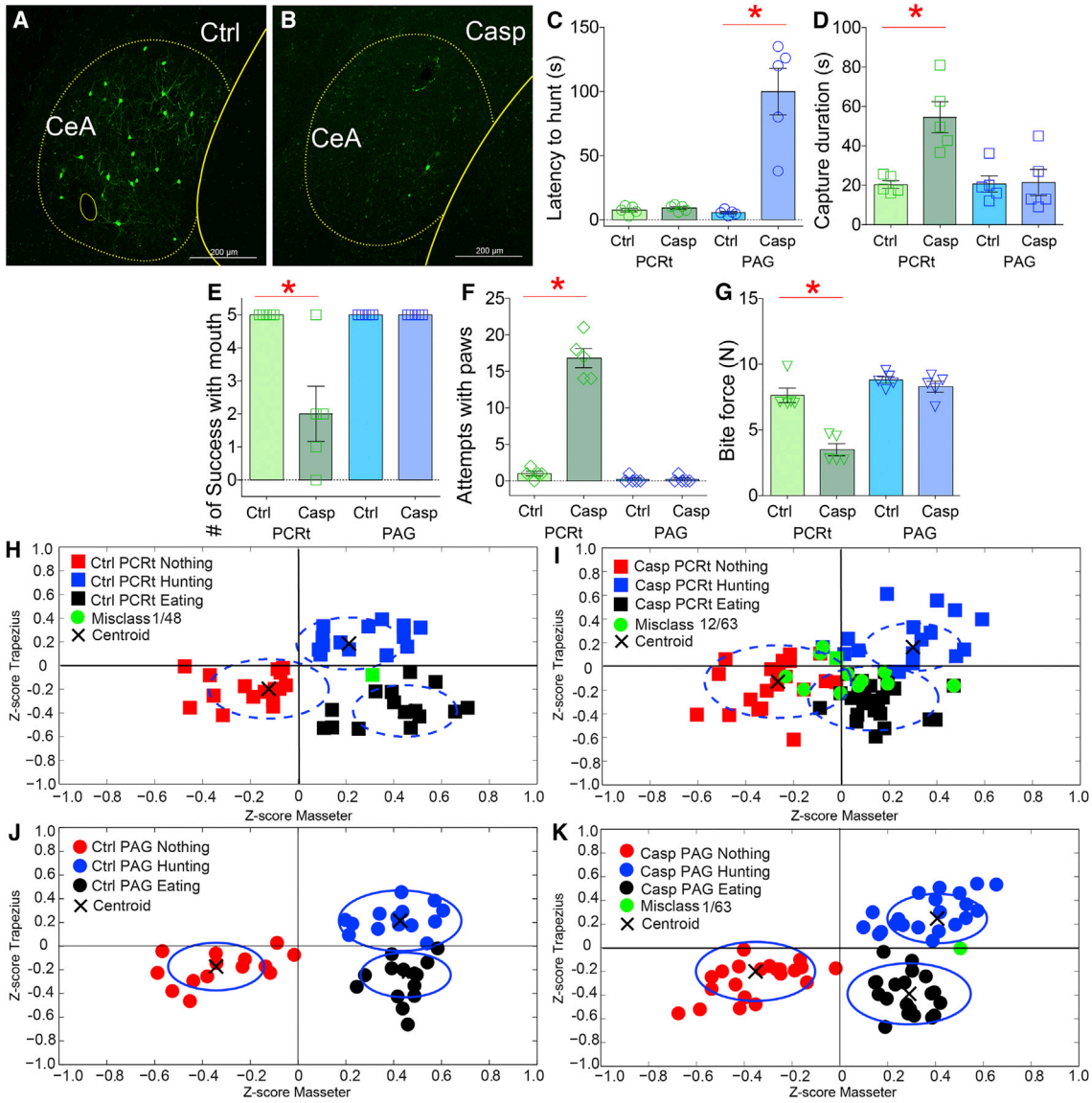

Figure 7. Pathway-Defined Lesions to Central Amygdala Neurons Differentially Impair Hunting

Two different groups of wild-type mice were transfected with the retrograde CAV2-*Cre*-GFP construct into PCRt or PAG. CeA was then transfected with *Cre*-inducible AAV-caspase. Two groups of control mice were also injected CAV2-*Cre*-GFP construct into PCRt or PAG, but CeA then transfected with *Cre*-inducible AAV-mCherry.

(A and B) Confocal images of CeA after CAV2-*Cre*-GFP injections into PCRt in control (A) and caspase-injected mice (B).

(C) Lesions to the CeA → PAG, but not to the CeA → PCRt, pathway caused dramatic increases in latencies to start pursuit ($n = 5$ per group, lesion × group effect $F[3,16] = 25.7$, $p < 0.001$; CeA → PAG Caspase group versus other groups, paired t test Bonferroni all $^*p < 0.001$).

(D) Lesions to the CeA → PCRt, but not to the CeA → PAG, pathway caused decreased hunting efficiency (lesion × group effect $F[3,16] = 8.9$, $p < 0.001$; CeA → PCRt Caspase group versus other groups, paired t test Bonferroni all $^*p < 0.02$).

(E) Lesions to the CeA → PCRt, but not to the CeA → PAG, pathway caused fewer prey captures with mouth ($F[3,16] = 12.8$, $p < 0.001$; CeA → PCRt Caspase group versus other groups, paired t test Bonferroni all $^*p < 0.01$).

(F) Lesions to the CeA → PCRt, but not to the CeA → PAG, caused frequent attempts to capture with forepaws ($F[3,16] = 139.2$, $p < 0.001$; CeA → PCRt Caspase group versus other groups, paired t test Bonferroni all $^*p < 0.001$).

(G) Lesions to the CeA → PCRt, but not to the CeA → PAG, pathway caused decreased incisor bite forces ($F[3,16] = 31.2$, $p < 0.001$; CeA → PCRt Caspase group versus other groups, paired t test Bonferroni all $^*p < 0.001$).

(H–K) *Z* scores from electromyogram patterns associated with behavioral events observed during the hunting sessions (classified as either "hunting prey"/"eating prey"/"other behavior (Nothing)") were plotted on the two-dimensional masseter × trapezius space. In the two groups of control mice (H and J), as well as in the CeA → PAG Caspase group (K), unsupervised algorithms efficiently assigned events of each type to the same cluster, i.e., rarely incurring in misclassifications

(legend continued on next page)

CeA → PCRt pathways combined led mice to robustly initiate predatory attacks on artificial prey (Figures 6C, 6D, and S6D–S6G; Movie S2).

The hunting of live prey involves fewer biting attacks than hunting artificial prey, as one lethal bite generally suffices. Thus, the significant effects of the combined stimulation on pursuit velocities, latencies, and capture duration closely mimicked those produced by activating CeA → PAG alone (Figures 6E–6G). Interestingly, activation of CeA → PCRt alone caused animals to engage in fictive feeding even when in the presence of prey, which resulted in slower velocities and longer latencies and capture durations (Figures 5E–5G).

To confirm the results above, we transfected the PCRt and/or PAG of wild-type mice with a retrogradely transported, monosynaptic canine adenovirus carrying a *Cre*-GFP construct (CAV2-Cre, Junyent and Kremer, 2015). CeA was then transfected with *Cre*-inducible ChR2-mCherry and implanted with optical fibers (Figures 6H, 6I, and S6H–S6L). Overall, the effects observed in these three groups of mice (CAV2-*Cre* injected only into PCRt, only into PAG, or into both PAG+PCRt) closely mimicked those produced by the multi-optical fiber approach described above (Figures 6J–6L).

These activation studies allow for three related conclusions. First, the CeA → PAG pathway controls the decision to initiate prey pursuit (via reducing latencies to initiate pursuit). Second, CeA → PCRt neurons control mandibular-cervical coordination and produce fictive feeding. Third, the net effect of activating both pathways was to cause both a short-latency/faster pursuit and forceful biting attacks. This consistently led to reduced hunting durations.

Pathway-Defined Lesions to Central Amygdala Neurons Differentially Impair Skilled Hunting

Finally, we aimed at analyzing the effects of ablating CeA neurons projecting to PCRt or PAG. This was achieved by transfecting the PCRt or PAG of wild-type mice with CAV2-*Cre*. Next, CeA was transfected with the viral construct that induces *Cre*-dependent caspase expression.

CAV2-*Cre* transfection in target sites induced GFP expression patterns that were locally restricted to CeA, mainly at its rostral levels, a pattern markedly reduced by caspase application (Figures 7A, 7B, and S7A–S7P). In contrast, caspase injections neither affected PCRt- or PAG-projecting neurons in hypothalamus nor overall neuronal survival in CeA (Figures S7Q–S7T).

Pathway-specific lesions revealed clear functional dissociations between the two CeA subpopulations. Lesions to the CeA → PAG pathway produced an ~10-fold lengthening in the latencies to pursue prey; in contrast, no latency effects were observed after lesions to the CeA → PCRt pathway (Figure 7C). Velocities during pursuit were only moderately affected by lesions to the CeA → PAG pathway (Figure S7U; intriguingly, these patterns very closely match those produced by depolarizing MLR neurons upon CeA → PAG activation, see Figures 5K–5M). Conversely, lesions to the CeA → PCRt pathway produced a robust lengthening of the time needed to successfully capture prey after pursuit was initiated (Figure 7D). No effects on capture duration were observed after lesions to the CeA → PAG pathway, as these animals achieved capturing prey using their jaws once the delayed prey pursuit was initiated (Figure 7D).

The defects in capturing prey observed in CeA → PCRt ablated mice resulted from a conspicuous alteration in hunting strategy. When facing insect prey, control mice characteristically extended the neck, oriented the head toward the prey, and rapidly captured prey using coordinated movements of jaws and forepaws. Mice sustaining lesions to CeA → PCRt, in contrast, kept their head closer to the trunk and generally attempted to capture prey using the forepaws without any assistance from the jaws (Movie S7). In fact, mice sustaining lesions to CeA → PCRt, but not to CeA → PAG, frequently failed to capture prey using their jaws (Figures 7E and S7V). This was then paralleled by the frequent display of attempting prey capture only using forepaws (Figure 7F). Consistently, mice sustaining lesions to CeA → PCRt, but not to CeA → PAG, displayed debilitated incisor biting forces (the pair of teeth used to perforate live prey, Figures 7G and S7W).

Pathway-Defined Lesions to Central Amygdala Neurons Altered Electromyogram Markers of Predatory Hunting

Z scores from the electromyogram patterns recorded during the hunting sessions were plotted onto the two-dimensional masseter × trapezius space. In both control mice and mice sustaining lesions to CeA → PAG, unsupervised algorithms sharply separated hunting versus non-hunting events, i.e., rarely incurred in misclassifications (Figures 7J and 7K). In contrast, in mice sustaining lesions to CeA → PCRt, clustering was significantly less efficient, with ~20% of hunting events being assigned to extraneous clusters (Figure 7I). In other words, lesions to CeA → PCRt abolished the cervical-mandibular neuromuscular command deployed during predatory hunting (Figures S7X–S7MM).

DISCUSSION

Our findings imply the central amygdala (CeA) as a modular command system (Ewert et al., 1990; Kupfermann and Weiss, 1978) for predatory hunting. Via two independent set of descending projections, CeA controlled distinct behavioral modules associated with efficient predation.

From an anatomical standpoint, the CeA is ideally positioned to mediate predation in vertebrates. The CeA projects densely to the parvocellular reticular formation (Shammah-Lagnado et al., 1992; Swanson and Petrovich, 1998; Van Daele et al., 2011), which comprises both cervical and mandibular premotor populations (Tellegen and Dubbeldam, 1999). We found that this arrangement allows for CeA control over the delivery of lethal biting attacks upon prey. Interestingly, the parvocellular reticular

(represented by green square). Black crosses represent centroids. (I) In CeA → PCRt Caspase mice, clustering was significantly less efficient, with hunting and non-feeding behaviors being assigned to extraneous clusters (n = 5 per group, proportion of misclassified events in CeA → PCRt Controls versus CeA → PCRt Caspase mice, $\chi^2(1) = 7.58$, Bonferroni $p < 0.02$; for CeA → PAG Caspase versus CeA → PCRt Caspase mice, $\chi^2(1) = 10.1$, $p < 0.008$).
Data are reported as mean ± SEM. See also Figure S7 and Movie S7.

formation also contains triceps muscle premotor pools (Esposito et al., 2014), implying that this reticular circuitry may mediate prey capture via the coordinated action of craniofacial, cervical, and forelimb systems.

CeA also projects densely to the central gray, which we found to innervate and control the adjacent mesencephalic locomotor region (Skinner and Garcia-Rill, 1984). We found that via this innervation CeA exerts control over the decision to initiate prey pursuit—which is characterized by predator stalking and possibly running toward prey. These central gray projections to locomotor regions also constitute a descending pathway that is independent from projections recently found to mediate gray-matter-induced freezing and flight (Tovote et al., 2016). These parallel CeA projections to reticular formation and gray matter provide a long-sought tractable network model for the integration of locomotion with prey capture (Wainwright et al., 2008).

The pattern of afferent inputs to CeA also mirrors its critical role in predation. Glutamatergic afferents arising from cortical olfactory brain regions densely target the CeA (Shammah-Lagnado and Santiago, 1999). Visual and auditory inputs are also critical for prey detection in mice (Hoy et al., 2016). CeA neurons activated by such inputs may convey prey-associated sensory information to downstream premotor circuits. Incoming prey-specific sensory inputs, which are bypassed by optical and chemogenetic exogenous activations, must thus confer the goal-directedness nature of predation. Our model is thus consistent with the notion that CeA responds to incentive cues (Robinson et al., 2014)—such as the sight or smell of prey—which act to elicit appropriate motor actions.

The rodent CeA, including its downstream projections to the gray matter, has been traditionally linked to threat detection (Davis, 1998; LeDoux et al., 1988; Tovote et al., 2016). Surprisingly, we failed to observe any occurrences of freezing upon optical stimulation of CeA. This was corroborated by the robust activation of the trapezius upon CeA stimulation, as the flattening of neck electromyogram traces is a reliable manifestation of freezing in mice (Steenland and Zhuo, 2009). We should note, however, that our lesions preserved caudal aspects of CeA, including its capsular subnucleus. Consistently, more caudal subnuclei of CeA contain genetically defined populations whose activation both suppress feeding (Cai et al., 2014) and mimic threat-induced reactions (Janak and Tye, 2015). Moreover, and in sharp distinction to optical stimulation of medial amygdala (Hong et al., 2014), we failed to observe attacks toward conspecifics upon CeA stimulation. Such contrast is presumably due to dedicated projections to hypothalamic attack areas from the medial, but not the central, nucleus of the amygdala (Canteras et al., 1995; Motta et al., 2009).

Finally, we note that morphological transition from jawless to jawed vertebrates resulted in the reconfiguration of craniofacial systems, including the emergence of a separate shoulder girdle supporting distinctive cervical muscles (Trinajstic et al., 2013). The emergence of a neck therefore appears as a distinct innovation inherent to jawed vertebrates (Kuratani, 2013; Tada and Kuratani, 2015; Trinajstic et al., 2013). Such an arrangement strongly favors efficient predation (Montuelle et al., 2009). We thus speculate that the emergence of jawed vertebrates was met with equivalent reconfigurations of amygdalar systems. Consistently, only the jawless lamprey appears to lack a differentiated "striatal" amygdala (Maximino et al., 2013), i.e., a CeA-homologous, peptide-rich structure within the amygdalar complex. Developmental genetic studies may determine the extent to which the emergence of a striatal amygdala constitutes an evolutionary novelty linked to the appearance of cervical-mandibular muscles.

STAR★METHODS

Detailed methods are provided in the online version of this paper and include the following:

- KEY RESOURCES TABLE
- CONTACT FOR REAGENTS AND RESOURCE SHARING
- EXPERIMENTAL MODEL AND SUBJECT DETAILS
  - Experimental Animals
- METHOD DETAILS
  - Stereotaxic viral injections and optical fiber implantation
  - Retrograde tracing from cranial and cervical muscles
  - Histological procedures
  - C-Fos measurements
  - Electromyogram electrodes, recordings, and analyses
  - In vivo electrophysiological recordings
  - Slice electrophysiology
  - Behavioral Studies
  - Food intake during optogenetics and Chemogenetic stimulation
  - Open field tests
  - Pellet reaching task
  - Locomotion test
  - Measurement of incisor bite forces
- QUANTIFICATION AND STATISTICAL ANALYSIS
  - Analysis of behavioral trials
  - Analysis of in-vivo electrophysiological data
  - Analysis of in-vivo electromyogram data
- DATA AND SOFTWARE AVAILABILITY

SUPPLEMENTAL INFORMATION

Supplemental Information includes seven figures, eight tables, and seven movies and can be found with this article online at http://dx.doi.org/10.1016/j.cell.2016.12.027.

AUTHOR CONTRIBUTIONS

I.E.d.A. conceived the study. I.E.d.A. and W.H. designed the experiments. W.H., L.A.T., M.J.R., and S.C.M. performed stereotaxic surgeries and behavioral, electromyogram, and optogenetic experiments and analyzed data. W.H., M.J.R., S.C.M., S.J.S.-L., and N.S.C. performed histological analysis and imaging. X.Z. and A.N.v.d.P. performed whole-cell patch-clamp experiments and analyzed data. W.H., L.A.T., and I.O.P. performed in vivo electrophysiological experiments and analyzed electromyogram and electrophysiological data. I.E.d.A. wrote the manuscript. All of the authors actively participated in interpreting all data and in manuscript editing.

ACKNOWLEDGMENTS

The authors thank the J. Buckley and Pierce Workshop for bite force device. This work was supported by the J.B. Pierce Laboratory, US National Institutes

of Health grants R01DC014859 and R01CA180030 (to I.E.d.A.) and R01 DK103176, DK084052, and NS48476 (to A.N.v.d.P.) and the National Natural Science Foundation of China 81671014 (to W.H.), Brazilian Government foundations FAPESP (2012/24679-0 to S.C.M. and 2014/26742-6 to M.J.R.) and CNPq (to N.S.C.).

Received: June 11, 2016
Revised: October 15, 2016
Accepted: December 15, 2016
Published: January 12, 2017

REFERENCES

Borghuis, B.G., and Leonardo, A. (2015). The role of motion extrapolation in amphibian prey capture. J. Neurosci. *35*, 15430–15441.

Butler, K. (1973). Predatory behavior in laboratory mice: strain and sex comparisons. J. Comp. Physiol. Psychol. *85*, 243–249.

Cai, H., Haubensak, W., Anthony, T.E., and Anderson, D.J. (2014). Central amygdala PKC-δ(+) neurons mediate the influence of multiple anorexigenic signals. Nat. Neurosci. *17*, 1240–1248.

Canteras, N.S., Simerly, R.B., and Swanson, L.W. (1995). Organization of projections from the medial nucleus of the amygdala: a PHAL study in the rat. J. Comp. Neurol. *360*, 213–245.

Catania, K.C. (2012). Evolution of brains and behavior for optimal foraging: a tale of two predators. Proc. Natl. Acad. Sci. USA *109* (*Suppl 1*), 10701–10708.

Comoli, E., Ribeiro-Barbosa, E.R., Negrão, N., Goto, M., and Canteras, N.S. (2005). Functional mapping of the prosencephalic systems involved in organizing predatory behavior in rats. Neuroscience *130*, 1055–1067.

Davis, M. (1998). Are different parts of the extended amygdala involved in fear versus anxiety? Biol. Psychiatry *44*, 1239–1247.

Esposito, M.S., Capelli, P., and Arber, S. (2014). Brainstem nucleus MdV mediates skilled forelimb motor tasks. Nature *508*, 351–356.

Ewert, J.P., Framing, E.M., Schürg-Pfeiffer, E., and Weerasuriya, A. (1990). Responses of medullary neurons to moving visual stimuli in the common toad. I. Characterization of medial reticular neurons by extracellular recording. J. Comp. Physiol. A Neuroethol. Sens. Neural Behav. Physiol. *167*, 495–508.

Farr, T.D., and Whishaw, I.Q. (2002). Quantitative and qualitative impairments in skilled reaching in the mouse (Mus musculus) after a focal motor cortex stroke. Stroke *33*, 1869–1875.

Finlay, B.L., Sengelaub, D.R., Berg, A.T., and Cairns, S.J. (1980). A neuroethological approach to hamster vision. Behav. Brain Res. *1*, 479–496.

Gans, C., and Northcutt, R.G. (1983). Neural crest and the origin of vertebrates: A new head. Science *220*, 268–273.

Hong, W., Kim, D.W., and Anderson, D.J. (2014). Antagonistic control of social versus repetitive self-grooming behaviors by separable amygdala neuronal subsets. Cell *158*, 1348–1361.

Hoy, J.L., Yavorska, I., Wehr, M., and Niell, C.M. (2016). Vision drives accurate approach behavior during prey capture in laboratory mice. Curr. Biol. *26*, 3046–3052.

Janak, P.H., and Tye, K.M. (2015). From circuits to behaviour in the amygdala. Nature *517*, 284–292.

Junyent, F., and Kremer, E.J. (2015). CAV-2–why a canine virus is a neurobiologist's best friend. Curr. Opin. Pharmacol. *24*, 86–93.

Kupfermann, I., and Weiss, K.R. (1978). The command neuron concept. Behav. Brain Sci. *1*, 3–39.

Kuratani, S. (2012). Evolution of the vertebrate jaw from developmental perspectives. Evol. Dev. *14*, 76–92.

Kuratani, S. (2013). Evolution. A muscular perspective on vertebrate evolution. Science *341*, 139–140.

Land, B.B., Narayanan, N.S., Liu, R.J., Gianessi, C.A., Brayton, C.E., Grimaldi, D.M., Sarhan, M., Guarnieri, D.J., Deisseroth, K., Aghajanian, G.K., and Di-Leone, R.J. (2014). Medial prefrontal D1 dopamine neurons control food intake. Nat. Neurosci. *17*, 248–253.

LeDoux, J.E., Iwata, J., Cicchetti, P., and Reis, D.J. (1988). Different projections of the central amygdaloid nucleus mediate autonomic and behavioral correlates of conditioned fear. J. Neurosci. *8*, 2517–2529.

Madisen, L., Mao, T., Koch, H., Zhuo, J.M., Berenyi, A., Fujisawa, S., Hsu, Y.W., Garcia, A.J., 3rd, Gu, X., Zanella, S., et al. (2012). A toolbox of Cre-dependent optogenetic transgenic mice for light-induced activation and silencing. Nat. Neurosci. *15*, 793–802.

Mallatt, J. (2008). The origin of the vertebrate jaw: neoclassical ideas versus newer, development-based ideas. Zoolog. Sci. *25*, 990–998.

Maximino, C., Lima, M.G., Oliveira, K.R., Batista, Ede.J., and Herculano, A.M. (2013). "Limbic associative" and "autonomic" amygdala in teleosts: a review of the evidence. J. Chem. Neuroanat. *48-49*, 1–13.

Montuelle, S.J., Herrel, A., Schaerlaeken, V., Metzger, K.A., Mutuyeyezu, A., and Bels, V.L. (2009). Inertial feeding in the teiid lizard Tupinambis merianae: the effect of prey size on the movements of hyolingual apparatus and the cranio-cervical system. J. Exp. Biol. *212*, 2501–2510.

Motta, S.C., Goto, M., Gouveia, F.V., Baldo, M.V., Canteras, N.S., and Swanson, L.W. (2009). Dissecting the brain's fear system reveals the hypothalamus is critical for responding in subordinate conspecific intruders. Proc. Natl. Acad. Sci. USA *106*, 4870–4875.

Nikulina, E.M. (1981). [Manifestations of predatory aggression in mice]. Zh. Vyssh. Nerv. Deiat. Im. I P Pavlova *31*, 1048–1053.

Robinson, M.J., Warlow, S.M., and Berridge, K.C. (2014). Optogenetic excitation of central amygdala amplifies and narrows incentive motivation to pursue one reward above another. J. Neurosci. *34*, 16567–16580.

Shaikh, M.B., Brutus, M., Siegel, H.E., and Siegel, A. (1985). Topographically organized midbrain modulation of predatory and defensive aggression in the cat. Brain Res. *336*, 308–312.

Shammah-Lagnado, S.J., and Santiago, A.C. (1999). Projections of the amygdalopiriform transition area (APir). A PHA-L study in the rat. Ann. N Y Acad. Sci. *877*, 655–660.

Shammah-Lagnado, S.J., Costa, M.S., and Ricardo, J.A. (1992). Afferent connections of the parvocellular reticular formation: a horseradish peroxidase study in the rat. Neuroscience *50*, 403–425.

Skinner, R.D., and Garcia-Rill, E. (1984). The mesencephalic locomotor region (MLR) in the rat. Brain Res. *323*, 385–389.

Stanek, E., 4th, Cheng, S., Takatoh, J., Han, B.X., and Wang, F. (2014). Monosynaptic premotor circuit tracing reveals neural substrates for oro-motor coordination. eLife *3*, e02511.

Steenland, H.W., and Zhuo, M. (2009). Neck electromyography is an effective measure of fear behavior. J. Neurosci. Methods *177*, 355–360.

Sternson, S.M., and Roth, B.L. (2014). Chemogenetic tools to interrogate brain functions. Annu. Rev. Neurosci. *37*, 387–407.

Swanson, L.W., and Petrovich, G.D. (1998). What is the amygdala? Trends Neurosci. *21*, 323–331.

Tada, M.N., and Kuratani, S. (2015). Evolutionary and developmental understanding of the spinal accessory nerve. Zoological Lett *1*, 4.

Tellegen, A.J., and Dubbeldam, J.L. (1999). Location of reticular premotor areas of a motor center innervating craniocervical muscles in the mallard (Anas platyrhynchos L.). J. Comp. Neurol. *405*, 281–298.

Tovote, P., Esposito, M.S., Botta, P., Chaudun, F., Fadok, J.P., Markovic, M., Wolff, S.B., Ramakrishnan, C., Fenno, L., Deisseroth, K., et al. (2016). Midbrain circuits for defensive behaviour. Nature *534*, 206–212.

Travers, J.B., and Norgren, R. (1983). Afferent projections to the oral motor nuclei in the rat. J. Comp. Neurol. *220*, 280–298.

Trinajstic, K., Sanchez, S., Dupret, V., Tafforeau, P., Long, J., Young, G., Senden, T., Boisvert, C., Power, N., and Ahlberg, P.E. (2013). Fossil musculature of the most primitive jawed vertebrates. Science *341*, 160–164.

Van Daele, D.J., Fazan, V.P., Agassandian, K., and Cassell, M.D. (2011). Amygdala connections with jaw, tongue and laryngo-pharyngeal premotor neurons. Neuroscience *177*, 93–113.

Wainwright, P.C., Mehta, R.S., and Higham, T.E. (2008). Stereotypy, flexibility and coordination: key concepts in behavioral functional morphology. J. Exp. Biol. *211*, 3523–3528.

Wickersham, I.R., Finke, S., Conzelmann, K.K., and Callaway, E.M. (2007). Retrograde neuronal tracing with a deletion-mutant rabies virus. Nat. Methods *4*, 47–49.

Yang, C.F., Chiang, M.C., Gray, D.C., Prabhakaran, M., Alvarado, M., Juntti, S.A., Unger, E.K., Wells, J.A., and Shah, N.M. (2013). Sexually dimorphic neurons in the ventromedial hypothalamus govern mating in both sexes and aggression in males. Cell *153*, 896–909.

STAR★METHODS

KEY RESOURCES TABLE

REAGENT or RESOURCE	SOURCE	IDENTIFIER
Antibodies		
Goat Anti-GFP antibody (FITC)	Abcam	Cat# ab6662; RRID: AB_305635
Anti-NeuN, clone A60 antibody	Millipore	Cat# MAB377; RRID: AB_2298772
Anti-c-Fos (Ab-5) (4-17) Rabbit pAb antibody	Millipore	Cat# PC38; RRID: AB_2106755
Rhodamine (TRITC)-AffiniPure Goat Anti-Mouse IgG (H+L)	Jackson ImmunoResearch Labs	Cat# 115-025-166; RRID: AB_2338490
Biotinylated Goat Anti-Rabbit IgG antibody	Vector Laboratories	Cat# BA-1000; RRID: AB_2313606
Chemicals, Peptides, and Recombinant Proteins		
FluoroGold (FG)	Manufacturer: Fluorochrome Inc; Purchased from Fisher scientific	Cat# NC0560981
Cholera Toxin B Subunit TRITC (CTB)	Manufacturer: List Biological Laboratories Inc; Purchased from Fisher scientific	Cat # 50-101-8773
Clozapine N-oxide (CNO)	Enzo Life Sciences, Inc.	Cat # BML-NS105-0025
Critical Commercial Assays		
VECTASTAIN Elite ABC HRP Kit (Peroxidase, Standard)	Vector Laboratories	Cat# PK-6100
Experimental Models: Organisms/Strains		
Mouse: C57BL/6J	The Jackson Laboratory	JAX: 000664
Mouse: Slc32a1$^{tm2(cre)Lowl}$/J	The Jackson Laboratory	JAX: 016962
Mouse: Slc17a6$^{tm2(cre)Lowl}$/J	The Jackson Laboratory	JAX: 016963
Mouse: Slc32a1^{tm1Lowl}/J	The Jackson Laboratory	JAX: 012897
Mouse: B6;129S6-Chat$^{tm2(cre)Lowl}$/J	The Jackson Laboratory	JAX: 006410
Mouse: B6;129P2-Gt(ROSA) 26Sor$^{tm1(CAG-RABVgp4,-TVA)Arenk}$/J	The Jackson Laboratory	JAX: 024708
Recombinant DNA		
AAV5-CMV-GFP	University of North Carolina's Vector Core	N/A
AAV5-CMV-Cre-GFP	University of North Carolina's Vector Core	N/A
AAV5-hSyn-hChR2(H134R)-EYFP	Dr. Karl Deisseroth-University of North Carolina's Vector Core	N/A
AAV5-EF1a-DIO-hChR2(H134R)-EYFP	Dr. Karl Deisseroth-University of North Carolina's Vector Core	N/A
AAV-EF1a-DIO-eArch3.0-EYFP	Dr. Karl Deisseroth-University of North Carolina's Vector Core	N/A
AAV5-EF1a-DIO-EYFP	Dr. Karl Deisseroth-University of North Carolina's Vector Core	N/A
AAV5-hSyn-DIO-hM3D(Gq)-mCherry	Dr. Bryan Roth - University of North Carolina's Vector Core	N/A
AAV5-hSyn-DIO-hM4D(Gi)-mCherry	Dr. Bryan Roth - University of North Carolina's Vector Core	N/A
AAV5-hSyn-DIO-mCherry	Dr. Bryan Roth - University of North Carolina's Vector Core	N/A
AAV5-hSyn-HA-hM3D(Gq)-IRES-mCitrine	Dr. Bryan Roth - University of North Carolina's Vector Core	N/A
AAV5-flex-taCasp3-TEVp	Dr. Nirao Shah - University of North Carolina's Vector Core	N/A

(*Continued on next page*)

Continued

REAGENT or RESOURCE	SOURCE	IDENTIFIER
AAV5-CA-FLEX-RG	Dr. Naoshige - UchidaUniversity of North Carolina's Vector Core	N/A
AAV5-EF1a-FLEX-TVA-mCherry	Dr. Naoshige – University of North Carolina's Vector Core	N/A
AAV-EF1a-DIO-Synb-eGFP	Ralph DiLeone Lab /Yale University (Land et al., 2014)	N/A
Pseudo-typed rabies construct EnvA G-deleted Rabies-EGFP	Salk Institute's Gene Transfer, Targeting and Therapeutics Core (GT3). (Wickersham et al., 2007)	N/A
CAV2-Cre-GFP	Institut de Génétique Moléculaire de Montpellier, France (Junyent and Kremer, 2015)	N/A
Software and Algorithms		
MATLAB R20 14a	MathWorks	https://www.mathworks.com/products/matlab/
Offline Sorter	Plexon	www.plexon.com/products/offline-sorter
PatchMaster 2.20	HEKA	http://www.heka.com/index.html
Igor Pro 6.36	WaveMetrics	https://www.wavemetrics.com/
EthoVision XT 11.5	Noldus	http://www.noldus.com/animal-behavior-research/products/ethovision-xt
LabView 2014	LabView	http://www.ni.com/download/labview-development-system-2014/4735/en/
GraphPad Prism 7	GraphPad	http://www.graphpad.com/scientific-software/prism/
Adobe design standard CS6	Adobe	http://shop.adobe.com/store/adbehme/en_IE/pd/ThemeID.29250800/productID.249257000
SPSS 21.0	IBM Predictive Software	https://www.ibm.com/support/knowledgecenter/SSLVMB
Other		
Implantable Optical Fibers	Doric Lenses, Canada	MFC_200/240-0.22_6mm_ZF1.25(G)_FLT
Formvar-Insulated Nichrome Wires (EMG recording)	A-M system	Cat # 762000
Male Miniature Pin Connector Fits Model 1800 / 3000 Headstage Leads (EMG recording)	A-M system	Cat # 520200
Female Miniature Pin Connector Fits A-M Systems' electrodes (EMG recording)	A-M system	Cat # 520100
16 tungsten microwires, 35-μm diameter (Electrophysiological recordings)	TDT systems	Cat # OMN1005
MATLAB script for electromyogram detection	de Araujo lab	https://www.dropbox.com/sh/6b3y7ult47m8mje/AAANdvXSwj2-iT39AP41kHQ1a?dl=0
MATLAB script for PCA calculation of neuronal data	de Araujo lab	https://www.dropbox.com/sh/ei2o6hdcqp4t8zf/AABnzqg5_eRE9Pp0oo16DfTQa?dl=0
Custom LabView-based computer interface (Measurement of biting forces)	John B Pierce Lab workshop	https://www.dropbox.com/sh/6iuocj9i8k5ziiv/AADyHz3yOeg7kNTXalgdoJoWa?dl=0

CONTACT FOR REAGENTS AND RESOURCE SHARING

Further information and requests for reagents should be directed to, and will be fulfilled by the Lead Contact Ivan E de Araujo (iaraujo@jbpierce.org, ivan.araujo@yale.edu).

EXPERIMENTAL MODEL AND SUBJECT DETAILS

All experiments presented in this study were conducted according to the animal research guidelines from NIH and were approved by the Institutional Animal Care and Use Committee of The J.B. Pierce Laboratory.

Experimental Animals

A total of 176 adult male mice were used. Strain details and number of animals in each group are as follows:

85 VGat-ires-*Cre* (Slc32a1$^{tm2(cre)Lowl}$/J (Jackson Laboratories stock #016962)
30 VGlut2-ires-*Cre* (Slc17a6$^{tm2(cre)Lowl}$/J (Jackson Laboratories stock #016963)
14 VGat-*floxed* (Slc32a1^{tm1Lowl}/J (Jackson Laboratories stock #012897)
6 Chat-ires-*Cre* × RΦGT = Chat-*Cre* (B6;129S6-Chat$^{tm2(cre)Lowl}$/J (Jackson Laboratories stock #006410)
× RΦGT (B6;129P2-Gt(ROSA)26Sor$^{tm1(CAG-RABVgp4,-TVA)Arenk}$/J (Jackson Laboratories stock #024708)
41 C57BL/6J (Jackson Laboratories stock #000664).

All mice used in experiments were individually housed under a 12 hr light/dark cycle. At the time of the experiments, animals were 8–20 weeks old. Littermates of the same sex were randomly assigned to experimental groups. Animals weighted approximately 25-28 g. All animals were used in scientific experiments for the first time. This includes no previous exposures to pharmacological substances or altered diets. The only pre-experimental intervention was acclimation to crickets, where all mice were food restricted for two consecutive dark cycles (2.5gram of food chow) and presented with five crickets for hunting habituation. All animals captured and consumed all crickets during habituation. Health status was normal for all animals.

METHOD DETAILS

Stereotaxic viral injections and optical fiber implantation

For all details on viral and tracer injections for each mouse strain, see Tables S1–S8. In all cases, preoperative analgesia: 5mg/Kg Carprofen (i.p.), anesthetic: 2% Isoflurane throughout, postoperative analgesia: 30mg/Kg Ibuprofen (in drinking water). Injections were performed with a Hamilton 1.0μL Neuros Model 7001KH syringe. Tables provide details for each strain separately. We list the viral construct/tracer injected, the relevant stereotaxic coordinates, and when applicable the relevant stereotaxic coordinates for optical fiber implants. When optogenetic and chemogenetics and/or caspase lesions were combined, the relevant constructs and coordinates are also listed on the same cell. Optical fibers were obtained from Doric Lenses Inc., and outer diameter is 240 μm; core diameter is 200 μm; numerical aperture is 0.22. Stereotaxic coordinates are with respect to bregma, according to standardized atlases of the mouse brain.

Retrograde tracing from cranial and cervical muscles

Mouse strain Chat-Cre × RΦGT

Mo5 (AP-5.1 mm, ML: 1.5mm, DV: −5.0mm) was injected unilaterally with SAD-ΔG-GFP 0.5μL. Appropriate location of viral injections was confirmed by injecting the Masseter with 1% FG 10μL, 0.5μL/min. 11N was also injected unilaterally with SAD-ΔG-GFP 0.5μL. To correctly target 11N, the mouse head was lowered; the skin open and blunt dissection of the cervical muscles exposed the cruciate ligament of atlas between the occipital bone and the first cervical vertebra. Ligament was adjusted to horizontal level. 0.5 μL SAD-ΔG-GFP was then injected 2.0mm caudal to the occipital bone, lateral 0.4mm from the midline, ventral 1.7mm from the ligament. Appropriate location of viral injections was confirmed by injecting the Trapezius: 1% FG 10μL, 0.5μL/min. 3 mice for Mo5 and 3 mice for 11N were used.

Histological procedures

Mice were deeply anesthetized with a ketamine/xylazine mix (400 mg ketamine + 20 mg xylazine kg body weight−1 I.P.). All animals were perfused with filtered saline, followed by 4% paraformaldehyde. Following perfusion, brains were left in 4% paraformaldehyde for 24 hr and then moved to a 20% sucrose solution in 0.02 M potassium phosphatebuffer (KPBS, pH 7.4) for 2 days. Brains were then frozen and cut into four series 40 μm sections with a sliding microtome equipped with a freezing stage. To identify fiber and electrode locations, relevant sections were identified and mounted on slides. Sections were then photographed under bright field and fluorescence. For SynaptoBrevin visualization, 4 weeks after viral injection, mice were perfused and brains cut at 40μm. The GFP signal was amplified with Goat Anti-GFP antibody (FITC), (ab6662, Abcam, 1:500). For SynaptoBrevin experiments combined with FluoroGold muscle injections, seven days after muscle injections animals were perfused as above and brains sliced in 40μm sections. For

verifying the extension of caspase-induced lesions, slices were incubated with Mouse Anti-Neuronal Nuclei (NeuN, MAB377, Millipore, 1:500) followed by TRITC-conjugated affinipure goat anti-mouse (IgG(H+L) 15-025-166, Jackson Immuno, 1:200). For visualizing FG/CTb dual injections, eight days after the injections, perfuse and slices the brain for 40μm. For visualization of rabies expression, ten days after the rabies injections, animals were perfused and expression was observed in coronal sections at ~160 μm intervals. Visualized cells were overlaid on a mouse brain atlas template.

C-Fos measurements

For determining the effects of optical stimulation on PCRt neuronal activity, unilateral 20Hz stimulation was performed using 10 s-long ON(0.02 s on/0.03 s off cycles were used during the ON cycles)/10 s-long OFF cycles for 10 min. For determining the combined effects of optically activating CeA and concomitantly chemogenetically activating PCRt, 10mg/Kg CNO i.p. were injected 10 min before the CeA 1Hz laser stimulation. Unilateral 1Hz stimulation was performed using 10 s ON (0.5 s on/0.5 s off cycles were used during the ON cycles)/10 s OFF cycles for 10 min. 90 min after the appropriate stimulation, mice were sacrificed and perfused as described before. To visualize Fos immunoreactivity, the ABC/DAB procedure was used. Briefly, brain sections were incubated with Rabbit Anti-c-Fos antibody (PC38, Calbiochem, 1:10000) (Concentration 1:10000), followed with Biotinylated Goat Anti-Rabbit IgG Antibody (BA-1000, Vector Laboratories, 1:200), then reacted with avidin-biotin-peroxidase complex ("ABC" method, Vectastain Elite ABC kit, Vector Laboratories, 1:200). A nickel diaminobenzidine (Nickel-DAB) glucose oxidase reaction was used to visualize Fos-like immunoreactive cells. Fos expression was analyzed and quantified as follows: Coronal sections at ~160 μm intervals in PCRt near the fiber implantation or Gq injection were photographed at 10 × magnification and montaged with Adobe Photoshopto to preserve anatomical landmarks. Fos+ neurons were counted manually on each slice (3 slices per animal) and expressed as the cumulative sum of Fos+ neurons within the relevant regions for each animal.

Electromyogram electrodes, recordings, and analyses

First, two twisted Formvar-Insulated Nichrome Wires (Diameter: Bare 0.002 inch. A-M system) were covered with polyethylene tubing (PE20, 0.15" x 0.45," Braintree scientific). The tips of the nichrome wires were bared and exposed. One bare wire tip was soldered to a Male Miniature Pin Connector (520200, A-M Systems). The other bare wire tip was inserted through a 30G needle, and the tip bent and used for the implants into the trapezius or masseter muscles. For implants, preoperative analgesia consisted of 5mg/Kg Carprofen, anesthetic was 2% Isoflurane throughout and postoperative analgesia, 30mg/Kg Ibuprofen. The skin of cheek was shaved and open to expose the masseter, or the skin on the back of the neck was open to expose the trapezius. The needle was then used for insertion of the wire into the muscle, with the bare wire hooked into the muscle. A suture was used to fix the wire in place. Skin was closed and a cemented miniature screw inserted into the parietal bone for fixating the remaining the polyethylene. Recordings were performed using the electromyogram module of a multichannel acquisition processor (Tucker-Davis Technologies, 3052Hz sampling rate). The male pin connector was attached to the female connector, which had been soldered to a recording headstage. Laser pulses timestamps were synchronized to the recordings via external TTL pulses into the TDT system. EMG signals from masseter and trapezius were recorded simultaneously in the same animals.

In vivo electrophysiological recordings

For array implantation *C57BL6/J* mice (N = 5) were placed on the stereotaxic apparatus and one electrode array consisting of 16 tungsten microwires (35-μm diameter, OMN1005, TDT systems) was implanted onto CeA (AP:-0.9mm ~1.4mm ML: 2.5mm ~2.7mm DV:-4.8mm). Locations of electrodes were confirmed histologically. Recordings were performed in combination with masseter recordings by simultaneously using the spike and EMG modules of the multichannel acquisition processor (Tucker-Davis Technologies). Previous to the neuronal and electromyogram recording sessions, mice were connected to commutators with flexible cables for habituation to recording conditions for one training session.

Slice electrophysiology

On the day of the experiments, VGat-*Cre* mice with selective ChR2 expression in CeA or PCRt neurons were anesthetized with isoflurane and decapitated for electrophysiological identification of ChR2-expressed neurons and circuit mapping. Brains were quickly removed and immersed in an ice-cold high-sucrose solution containing (in mM): 220 sucrose, 2.5 KCl, 6 MgCl2, 1 CaCl2, 1.23 NaH2PO4, 26 NaHCO3, and 10 glucose (gassed with 95% O2 / 5% CO2; 300-305 mOsm). Coronal brain slices 300 μm thick were sectioned using a vibratome. Brain slices were then transferred to an incubation chamber filled with an artificial CSF (ACSF) solution containing (in mM) 124 NaCl, 2.5 KCl, 2 MgCl2, 2 CaCl2, 1.23 NaH2PO4, 26 NaHCO3, and 10 glucose (gassed with 95% O2 / 5% CO2; 300-305 mOsm) at room temperature (22°C). After a 1-2 hr recovery period, slices containing CeA, PCRt, or PAG were selected and transferred to a recording chamber mounted on a BX51WI upright microscope (Olympus, Tokyo, Japan). The recording chamber was perfused with a continuous flow of gassed ACSF. A dual-channel heat controller (Warner Instruments, Hamden, CT) was used to control the temperature of recording solution at 33 ± 1°C. Whole-cell patch-clamp recordings were performed on neurons in CeA, PCRt or PAG that were visualized using an infrared-differential interference contrast (DIC) optical system combined with a monochrome CCD camera and a monitor. Pipettes were pulled from thin-walled borosilicate glass capillary tubes (length 75 mm, outer diameter 1.5 mm, inner diameter 1.1mm, World Precision Instruments) using a P-97 micropipette puller (Sutter Instruments, Novato, CA). Pipette solution containing (in mM) 145 K-gluconate, 1 MgCl2, 10 HEPES, 1.1 EGTA, 2 Mg-ATP, 0.5 Na2-GTP,

and 5 Na2-phosphocreatine (pH 7.3 with KOH; 290-295 mOsm) were used for whole-cell recording. The pipettes of resistances ranging from 3 to 6 MΩ were used for experiment. EPC-10 patch-clamp amplifier (HEKA Instruments, Bellmore, NY) and PatchMaster 2.20 software (HEKA Elektronik, Lambrecht/Pfalz, Germany) were used to acquire and analyze data. Pipette and cell capacitance were compensated during experiment and neurons for which the series resistance was > 20 MΩ were excluded from the statistics. Traces were processed using Igor Pro 6.36 (Wavemetrics, Lake Oswego, OR). Inhibitory postsynaptic currents were recorded at the holding potential of −40 mV unless otherwise mentioned. A 473 nm blue laser (Doric Lenses) was used to evoke the stimulation for optogenetic activation of ChR2 channels in brain slices. Continuous stimulation and stimulation of 10 ms duration with different frequency (1, 5, 10, 20 Hz or 1Hz, 500ms) were used in the experiment to test photostimulation-evoked response. For recording VGlut2+ neurons in PAG innervated by ChR2+ CeA afferents, VGlut2-ires-*Cre* mice transfected with AAV5-DIO-mCherry in PAG were used.

Behavioral Studies

Video scoring

All behavioral sessions were video-recorded using a high-speed (120fps) camera (DMC-FZ200, Panasonic). Video scoring was performed by extracting timestamps associated with the relevant behavioral events (which are listed below). Timestamp extraction made use of the CPU's clock during video execution and was obtained using custom software available upon request. A number of measurements, including overall locomotion and displacement velocity made use of automated video analyses (EthoVision XT11.5, Noldus).

Cricket hunting during optogenetics experiments

Mice, either fed ad libitum or food restricted (''deprived'' 2.5g chow/day), were placed in a clean empty cage for 30mins before the laser stimulation. 10 min before the laser stimulation, the cage was cleaned again, and at the beginning of each trial. The mouse was located on one corner of the cage whereas the cricket was released into the cage near the diagonally opposite corner. A stationary object or an artificial moving prey also was gently placed in the diagonally opposite corner of the cage. Stationary objects were one of the following: wood stick cut from applicators (diameter 0.15cm length 1.5cm (short) or 5cm (long)); Small bottle cap (1cm diameter, 0.6cm high); Tape roll (5cm diameter, 2.5cm high); Food pellet (3g of regular chow 5001, Labdiet); Soft pellet (3g of 24%Fat pellet D12451, Research Diets, Inc); Hard pellet (3g 35% Sucrose pellet, D12450B, Research Diets, Inc). The moving artificial prey was a miniature battery powered robot (HEXBUG Nano obtained from Amazon.com).

Optical Stimulation regimens

Stimulation frequencies were chosen according to the outcome of the slice electrophysiological studies. Although we did not detect major differences between stimulation frequencies in terms of evoking (or failing to) behavior, we used the following frequencies in each case. For CeA laser stimulation: 473-nm blue laser (or 532-nm green laser), stimulation was performed using 1min OFF - 1min ON (1Hz, 0.5 s on/0.5 s off cycles were used during the ON period) - 1min OFF cycle totaling 3 min.

PCRt/CeA = > PCRt or CeA = > PAG: 473-nm blue laser (or 532-nm green laser) stimulation was performed using 1min OFF - 1min ON (20Hz, 0.02 s on/0.03 s off cycles were used during the ON period) - 1min OFF cycle for totally 3 min.

House crickets (*Grillus domesticus*) were purchased from pet food providers (http://www.petco.com/shop/en/petcostore and http://www.flukerfarms.com/). All mice were habituated to hunt and eat crickets for two days before the test day. During habituation, the mice were 2.5g chow restricted, and presented with 5 crickets to hunt overnight. During the test, the mice were 2.5g chow restricted. Behaviors were digitally recorded with high-speed (120fps) camera (DMC-FZ200, Panasonic). Cricket specifications are as follows: large crickets, ~1 inch, 0.5g. Small crickets, ~0.5 inch, 0.1g. Experiments were performed on standard mouse home cages.

Behavioral parameters

Latency to hunt: time taken from mice fixating at the crickets until mice actually start the pursuit. Capture duration: time taken from mice starting to pursue the crickets until successfully capturing the crickets using either the fore-paws or the mouth, not necessarily killing the crickets. Eating duration: time taken from mice capturing the crickets until mice stopped eating the crickets. Attempt with mouth: Mouse tries to capture the cricket only using biting or biting with forepaw assistance. Attempt with forepaw: Mouse tries to capture the cricket using only fore-paws. In every trial, once mice stopped eating the crickets, any insect residuals were removed, and another live cricket was then placed into the cage. All the experiments were repeated 5 times per animal and averages taken.

For the hunting data specifically shown in the *Results* section of the manuscript, the experimental conditions were as follows: *CeA stimulation:* Mice were either fed ad libitum satiated or food restricted at 2.5g chow/day. 1Hz laser. One cricket per trial. All the results shown correspond to averages over five trials.

Chemogenetic activation

Clozapine-N-Oxide (1mg/kg) was injected i.p. 10mins before the start of the hunting sessions.

Food intake during optogenetics and Chemogenetic stimulation

Mice were single caged and 2.5g chow/day food restricted. Soft food (chow) or hard food (High sugar pellet: #D12450B, Research Diet, USA) was placed in their home-cage at the same time of the day. After 1 hr free consumption, the pellets were removed and weighted. After 3 days of habituation with either laser cable connection or Saline i.p. injection, on the test day, the mice were exposed to laser (Laser cycle of 5min ON – 5min OFF for 1Hr. During the ON period, 473-nm blue stimulation was performed 1Hz of 0.5 s on/0.5 s off cycles.) or i.p injected with CNO (1mg/kg). The total food intake was weighted and the eating behavior video recorded for further analysis.

Open field tests

To assess locomotor activity in response to laser stimulation, animals were placed on a novel Plexiglas arena (Med Associates, 25 cm × 30 cm). The total area was divided into nine equal rectangular subareas (8.3 × 10 cm), demarcated with yellow tape. Immediately above the central subarea a 150-W lamp was activated to induce natural aversion to this particular location, as usually performed. Animals were tested once in this arena. The laser cycle was randomly chosen for 5min ON – 5min OFF or 5min OFF – 5min ON. During the ON period, 473-nm blue laser (or 532-nm green laser) stimulation was performed 1Hz of 0.5 s on/0.5 s off cycles. The sessions were digitally recorded with a Sony HDR-CX440 camera. Data were analyzed by replaying the sessions in slow motion. Outcomes were the number of sequential crossings over different adjacent yellow lines (representing total locomotor activity), and relative time spent within the illuminated central part of the arena.

Pellet reaching task

Mice were food-restricted to 2.5g/day. The training chamber was built from clear Plexiglas (4mm thickness; 30cm x 30cm x 30cm). One vertical slit (1 cm wide; 3-cm high) was located on the front wall of the box. Single reachable sugared food pellets (0.02 g, Bio-Serve) were located 1 cm away from the slit, on a platform of 1.5 cm height. Two photodetectors were located on either side of the platform; the centerline of the two photodetectors is 2mm above the pellet. After one day of habituation to the box without presentation of pellets outside the slit, the assay consisted of 2 phases: shaping and training. During the shaping phase (day 1), mice are allowed to reach for multiple pellets presented to them outside the box to determine the preferred limb. During the training phase (day 2–8), individual pellets are placed in front of the slit on the opposite side the preferred limb. When mice can reach 20 pellets within 10mins, we consider the mice learned the performance. For the test day, all the behaviors were recorded with two cameras (one in front of the slit and the other one beside the cage). Once the forepaw crosses the slit and touches the pellet, the photodetector will detect the movement and trigger the laser source via a programmed TTL pulse (20Hz, 0.02 s on/0.03 off cycles for 5 s). All mice performed 20 trials. The photodetector activated the laser source for every other presented pellet. The Reaching accuracy was determined using slow motion video surveillance according to 4 criteria: "miss" (no touch with the pellet during reach), "no grasp" (paw contact with pellet but no correct grasping), "drop" (the pellet is retrieved but falls before taking it into the mouth), "success" (the mouse retrieves the pellet directly to its mouth). Success rate was calculated as the percentage of successful reaches over total reaching attempts.

Locomotion test

Mice were either fed ad libitum satiated or food restricted at 2.5g chow/day, were connected to the laser cable and placed in a clean cage or home cage for 30mins before the laser stimulation.

CeA laser stimulation: 473-nm blue laser 1min (1Hz, 0.5 s on/0.5 s off cycles).
CeA = > PCRt/CeA = > PAG: 473-nm blue laser 1min (20Hz, 0.02 s on/0.03 s off cycles).

All behaviors were videotaped from above the cages. Videos were analyzed with Ethovision XT11.5 (Noldus). Parameters involved defining the arena, define mouse contour versus background contrast. Parameters extracted included distance covered, velocity and mobile frequency.

Measurement of incisor bite forces

Measurement of biting forces was obtained using an accurate single point load cell system (OEM Style Single Point Load Cells, Omega). The system was connected to a purpose-built, 3D-printed mouth piece whose dimensions (H = 1mm × W = 5mm) were based on incisor morphology of adult C57BL6/J mice. Output signals were digitized via a National Instruments board (NI USB-6009) and fed into a custom LabView v2014-based computer interface. Awake animals were restrained for the biting tests, as usually performed. Raw signals obtained during biting periods were averaged and entered into statistical analyses software. Our baseline measurements in control mice (~9-10N) closely match currently published values for healthy adult mice.

QUANTIFICATION AND STATISTICAL ANALYSIS

Data analyses, excluding all electromyogram/electrophysiological data, were performed using SPSS (v.21.0, IBM Predictive Software), Ethovision XT 11.5 (Noldus), GraphPad Prism 7 (GraphPad) and MATLAB (v.14a, MathWorks). Animals assigned to the different experimental groups were experimentally naive littermates, so that no randomization or other a priori criteria were adopted for group assignments. Experimental manipulations were analyzed according to within-subject repeated-measures designs. Order of experimental conditions was randomly assigned across subjects. Samples sizes were chosen based on our previous studies employing similar optogenetic, electrophysiological and neuronal ablation approaches. Samples sizes adopted in our current study were sufficient for detecting strong effect sizes while complying with guidelines from local enforcing rules requesting minimal animal usage by J.B. Pierce's Institutional Animal Care and Use Committee. Experimenters were not blind to experimental conditions. Only animals carrying signs of distress/infection/bleeding/anorexia after the surgical procedures were excluded. Data from all animals used in the experiments were included in the final analyses and plots.

Analysis of behavioral trials

For all behavioral studies, including those resulting from pathway-targeted lesions, optogenetics and/or chemogenetic experiments, analyses made use of standard linear models (Pearson correlation), as well as one- or two-way (repeated-measures) ANOVAs and post hoc t tests tests whenever relevant, for correcting for multiple comparisons. All data were reported as mean ± SEM. In all cases sample sizes (N) denote number of animals used. All p values associated with the t tests performed correspond to two-tailed tests, and all post hoc tests were corrected for multiple comparisons by employing Bonferroni correction. To assess potentially spurious results associated with non-normality, all significant effects were confirmed by rerunning the tests using the appropriate non-parametric test. All data are individually plotted (Prism 7, GraphPad), and the corresponding bar plot of the precision measures (mean ± SEM) were overlaid on the figure. The exact value of all N (always number of animals), df, T/F/ χ^2, and p values are reported in the figure legends. An effect was considered statistically significant whenever the corresponding statistic was associated with a p value (Bonferroni-corrected when appropriate) strictly less than 0.05.

Analysis of in-vivo electrophysiological data

61 single neurons displaying action potentials of signal-to-noise ratios > 3:1, were analyzed. Otherwise data were discarded. Data were pooled from five different C57BL6/J mice. The action potentials were isolated online by means of voltage-time threshold windows and a three-principal components contour templates algorithm. Spikes were resorted using the Offline Sorter software (Plexon). Data were then imported into MATLAB (v.14a, MathWorks) using custom-written software. To calculate firing rates, instantaneous firing rates were smoothed using MATLAB-based filtering with a 60 s moving average using 50ms bins. For all neurons recorded, the firing rates of peri-event epoch (i.e., hunting, prey capture, and eating) were arranged in a matrix (neurons = rows and bins = columns). The rows of the matrix were normalized as z-scores and then plotted using the corresponding first principal component. To test the significance of firing rate changes, we used an individual unit analysis. A non-parametric Wilcoxon signed-rank test was performed on each unit to determine whether the mean firing rate after the event (i.e., hunting, prey capture, and eating) was significantly different from baseline, and units were classified in three populations: Excited, Inhibited; or Neutral. Overall ensemble activity was calculated by averaging the firing rates of each classified population. The exact value of all N (always number of neurons), df, T/F/ χ^2, and p values are reported in the figure legends. An effect was considered statistically significant whenever the corresponding statistic was associated with a p value (Bonferroni-corrected when appropriate) strictly less than 0.05.

Analysis of in-vivo electromyogram data

To perform across-animal analyses of the signal amplitude, signals were full-wave rectified and root mean square (RMS)-converted within moving windows of 50-ms duration, and then standardized by calculating the z-scores. Z-scores were calculated based on the duration of the trials and used to: (*i*) estimate the relative EMG change in response to the presentation of different behavioral actions (i.e., hunting, pray capture and eating) and (*ii*) identify the number of EMG bursts by using a cut off of z score $\geq$ 2. Sample sizes (N) always denote number of trials pooled across six different C57BL6/J mice. To determine whether the mean amplitude signal after the event (e.g., hunting or prey capture) was significantly different from baseline, *Bootstrap* methods were used to randomize the distribution of z-scores around the event and compute the associated p value accordingly. For cluster analyses, the mean post-event z-score from each animal was plotted on a two-dimensional trapezius × masseter space, since the electromyograms were recorded simultaneously. An unsupervised K-means algorithm was then employed to determine the centroids based on the number of a priori experimental conditions involved in each case. These analyses were performed using custom software programmed in MATLAB (v.14a, MathWorks) and are available upon request. The exact value of all N (always number of trials), df, T/F/ χ^2, and p values are reported in the figure legends. An effect was considered statistically significant whenever the corresponding statistic was associated with a p value (Bonferroni-corrected when appropriate) strictly less than 0.05.

DATA AND SOFTWARE AVAILABILITY

Custom software are available. See Key Resources Table above for download details.

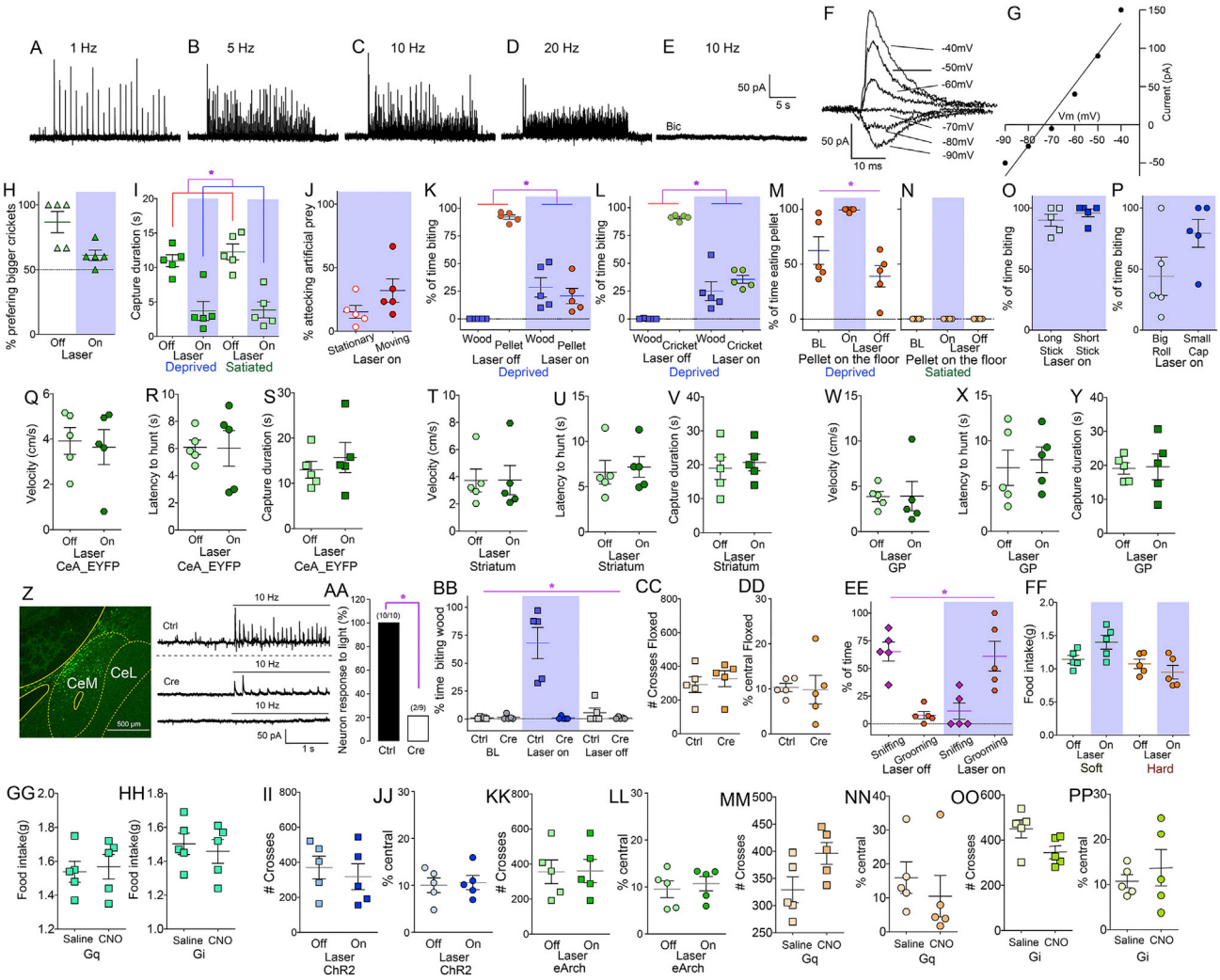

Figure S1. Characterization of the Effects Produced by Optically and Chemogenetically Activating Central Amygdala, Related to Figure 1

A–D. Photostimulation of CeA in slices using blue light at 1, 5, 10, 20Hz evoked outward postsynaptic currents in neighboring neurons lacking ChR2 expression. Membrane potentials were clamped at −40mV. E. Photostimulation-evoked outward postsynaptic currents were blocked in the presence of bicuculine (30 µM). F. Photostimulation with 10ms blue light evoked postsynaptic currents in neighboring CeA neurons at various holding potentials ranging from −90 mV to −40 mV. G. Linear current-voltage relationship shows reversal potentials of approximately −70mV, which is close to the equilibrium potential for Cl^- current which is determined by the Cl^- concentration in both ACSF and pipette solution. H. CeA optical activation did not reduce significantly the otherwise typical preferences for hunting larger, more nutritious prey (N = 5, main effect of laser on preference for larger prey, paired t test t[4] = 2.2, p = 0.084). Shaded blue area delimits laser on period. I. CeA optical activation significantly reduced the time needed for mice to successfully capture cricket prey, independently of internal state (N = 5, two-way RM ANOVA main effect of laser F[1,4] = 53.7, *p = 0.002). Shaded blue area delimits laser on period. J. CeA optical activation elicited predatory-like attacks on an artificial insect irrespective of its state (stationary versus moving, %time attacking prey, N = 5, t[4] = 2.4, p = 0.069). Shaded blue area delimits laser on period. K. CeA optical activation abolished normal preferences toward biting edible (food pellet) over inedible (wood stick) objects (N = 5, two-way RM ANOVA main effect of laser F[1,4] = 29.8, *p = 0.005; laser × edibility effect F[1,4] = 51.5, p = 0.002). Shaded blue area delimits laser on period. L. Same as in (K). CeA optical activation abolished normal preferences toward biting insects over inedible (wood stick) objects (N = 5, two-way RM ANOVA main effect of laser F[1,4] = 15.5, *p = 0.017; laser × edibility effect F[1,4] = 61.5, p = 0.001). Shaded blue area delimits laser on period. M-N. CeA optical activation increased food pellet biting in hungry (M), N = 5, laser effect on %time biting F[2,8] = 10.1, *p = 0.006) but not in sated mice (N), p ≈ 1.0). O-P. CeA optical activation led to biting of inedible objects irrespective of size (O), laser effect on %time biting long versus short wood sticks N = 5, paired t test t[4] = 2.4, p = 0.374; P. small versus large plastic bottle tops N = 5, t[4] = 2.1, p ≈ 0.1). Shaded blue area delimits laser on period. Q-Y. In control experiments for optogenetic stimulation we tested the effects of CeA optical activation on pursuit velocity, latency to pursue, and hunting efficiency (capture duration). None of these three parameters were affected by optical activation in VGat-ires-*Cre* mice transfected with a *Cre*-inducible AAV-EYFP (non-light excitable fluorophore) construct in CeA (panels (Q),(R),(S), paired t–test laser effect all p > 0.2); VGat-ires-*Cre* mice transfected with *Cre*-inducible AAV-ChR2 in lateral striatum neighboring CeA (panels (T),(U),(V), paired t–test laser effect all p > 0.7); VGat-ires-*Cre* mice transfected with *Cre*-inducible AAV-ChR2 in *globus pallidus* (panels (W),(X),(Y), paired t–test laser effect all p > 0.6). All groups N = 5. Z-EE. VGat-*floxed* mice were virally transfected with both *Cre* recombinase and non-*Cre*-dependent ChR2 into CeA. *Cre*-recombinase in VGat-*floxed* mice causes genetic ablation of VGat expression. Z. *Left* Expression of virally-delivered *Cre*-GFP (AAV-*Cre*-eGFP) in CeA of VGat-*floxed* mice. *Right* Representative trace (top) shows that photostimulation clearly increases IPSC frequency and amplitude on a CeA neuron after AAV-ChR2-EYFP and AAV-GFP

(legend continued on next page)

was injected to VGat-*floxed* mice to induce ChR2 expression in CeA neurons. Representative traces (bottom) show that either photostimulation only slightly increased IPSC frequency or produced no effect on a CeA neuron after AAV-ChR2-EYFP plus AAV-*Cre*-GFP were injected to CeA of VGat-*floxed* mice. AA. Bar graphs shows proportions (%) of CeA neurons that responded to photostimulation by increasing IPSCs in control (ctrl, black, injected with AAV-ChR2-EYFP and AAV-GFP) or VGat-ablated (cre, white, injected with AAV-ChR2-EYFP and AAV-Cre-GFP) VGat-*floxed* mice. N = 19, $\chi^2 = 12.3$, *p = 0.001. BB. The panel shows that VGat ablation from CeA completely abolished the ability of CeA optical stimulation to induce the grasping and biting of inedible objects (wood sticks). Control Vgat-*floxed* mice were transfected with non-*Cre*-dependent ChR2 and AAV-GFP (%time biting wood sticks, N = 5 each group, two-way RM ANOVA laser × *Cre*-induced recombination effect $F(2,16) = 24.63$, *p < 0.001). Shaded blue area delimits laser on period. CC. Open field tests reveal no effects of ablating VGat in CeA on locomotor activity in a novel arena (number of crossings through the arena's subregions, N = 5 in each group, two-sample t test t[8] = 0.5, p = 0.6). DD. Neither were detected differences in time spent within the illuminated central area of the arena (N = 5, t[8] = 0.15, p = 0.8). EE. CeA optical activation in male mice altered social behaviors toward adult females. When laser was OFF male mice investigated ("sniffed") the female's genital area while displaying few episodes of grooming. This relationship was inverted by laser activation (N = 5, two-way RM ANOVA laser × grooming versus investigation effect $F(1,4) = 49.8$, *p = 0.002). Importantly, aggressive attacks or biting of conspecifics were never observed. FF. CeA optical activation failed to alter intake of either soft (high-fat) or hard (low-fat) food pellets (N = 5, two-way RM ANOVA main effect of laser $F[1,4] = 2.0$, p = 0.2; laser × pellet type $F[1,4] = 3.6$, p = 0.129). GG-HH. Chemogenetic activation or inhibition of CeA neurons failed to alter food intake levels (N = 5, Excitation: panel GG, paired t–test CNO effect p > 0.6; N = 5, Inhibition: panel HH, paired t–test CNO effect p > 0.3). CNO = Clozapine-N-oxide, designer activator drug. II. Open field tests reveal no effects of CeA optical activation of ChR2 on locomotor activity in a novel arena (number of crossings through the arena's subregions, N = 5, laser effect paired t test t[8] = 0.29, p = 0.7). JJ. Neither were detected differences in time spent within the illuminated central area of the arena (t[4] = 0.22, p = 0.8). KK. Open field tests reveal no effects of CeA optical activation of eArch on locomotor activity in a novel arena (number of crossings through the arena's subregions, N = 5, two-sample t test t[4] = 0.04, p = 0.96). LL. Neither were detected differences in time spent within the illuminated central area of the arena (t[4] = 0.6, p = 0.5). MM-NN. Open field tests reveal no effects produced by chemogenetic activation of CeA neurons on locomotor activity in a novel arena (number of crossings through the arena's subregions, N = 5, paired t test p = 0.1). NN. Neither were detected differences in time spent within the illuminated central area of the arena (p = 0.1). OO-PP. Open field tests reveal no effects produced by chemogenetic inhibitionof CeA neurons on locomotor activity in a novel arena (number of crossings through the arena's subregions, N = 5, paired t test p = 0.3). NN. Neither were detected differences in time spent within the illuminated central area of the arena (p = 0.4). Data reported as mean ± SEM.

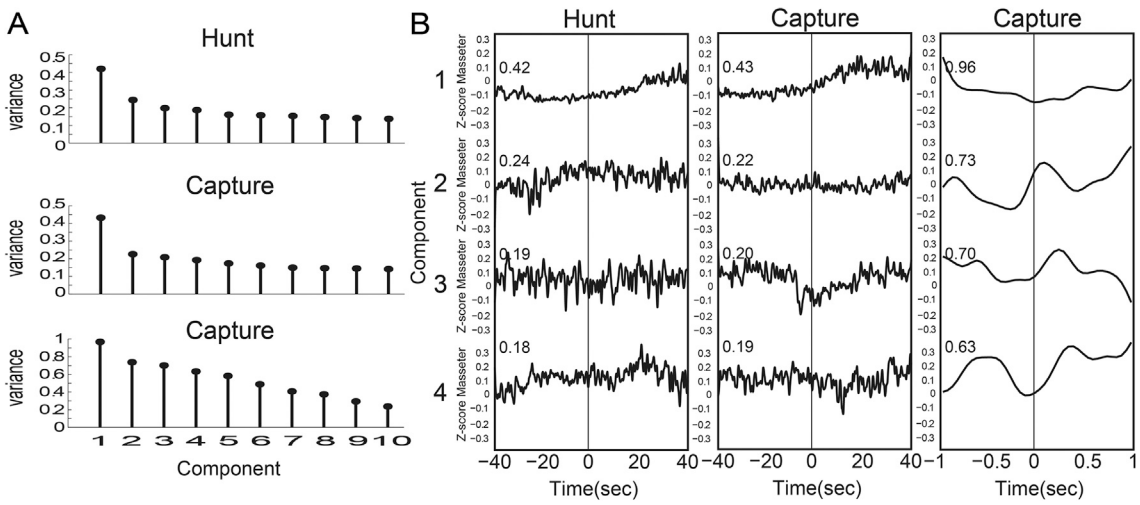

Figure S2. Principal Component Analyses of Predation-Responsive Neurons in Central Amygdala, Related to Figure 2

A. The plot displays the averages of variance accounted for the first ten Principal Components for neurons recorded in CeA during hunting (top, cf. Figure 1A), prey capture (middle, cf. Figure 1D) and capture at higher temporal resolution (bottom, cf. Figure 1G). B. Z-scores associated with the first four Principal Components for the same neurons recorded in CeA during hunting (left, cf. Figure 1A), prey capture (middle, cf. Figure 1D) and capture at higher temporal resolution (right, cf. Figure 1G). The numbers above each trace represent the variance accounted for in each case, as in A.

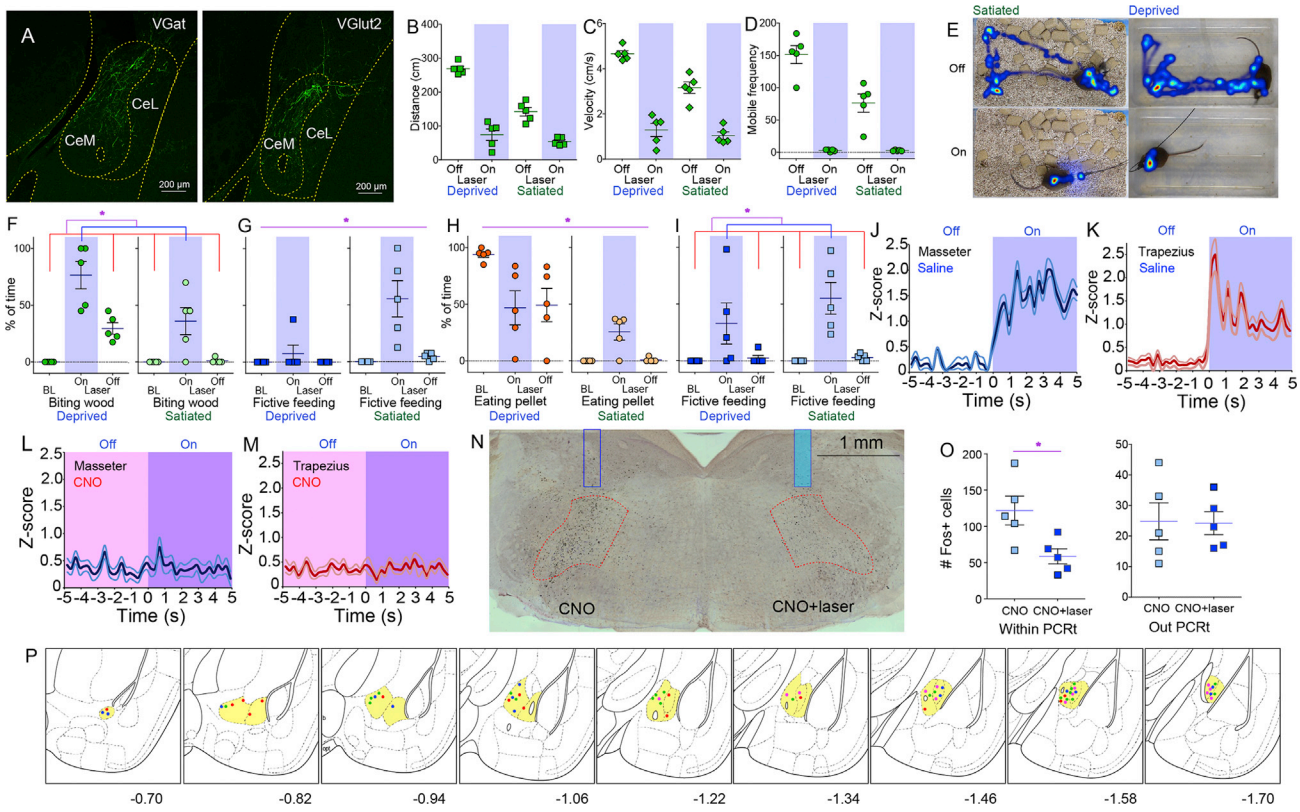

Figure S3. Functional Characterization of Central Amygdala Projections to the Parvocellular Reticular Formation, Related to Figure 3

A. *Cre*-dependent pseudotyped rabies virus SADΔG-GFP(EnvA) was injected in PCRt of VGat-ires-*Cre* (left) and VGlut2-ires-*Cre* (right) mice. The panel shows the extent of labeling in centromedial (CeM) and centrolateral (CeL) regions of CeA. The figures reveal that most rabies-labeled cells were located within CeM. Although detectable, fewer cells were located in CeL. See detailed distribution on panel (P) below. Note the absence of labeled cells in neighboring regions. B-E. Illustrative heatmaps from locomotion patterns observed upon CeA = > PCRt optical activation. Optical activation of CeA = > PCRt projections caused fictive feeding, leading to an arrest in locomotion concomitant to the sequence's execution. The effect occurred independently of internal state, but change was more conspicuous in the sated state (B: Distance: N = 5, two-way RM ANOVA laser × internal state effect $F[1,4] = 14.5$, *p = 0.019; C: Velocity: $F[1,4] = 15.1$, *p = 0.018; D: Mobile frequency: $F[1,4] = 11.0$, *p = 0.02; E: Illustrative locomotion heatmaps in home and empty cages, lower maps show effect of laser on. F. Frequency of biting inedible (wood stick) object induced by CeA = > PCRt optical activation, which was elicited in both hungry and sated states (N = 5 two-way RM ANOVA main effect of laser $F[2,8] = 31.9$, *p < 0.001). G. Frequency of fictive feeding induced by CeA = > PCRt optical activation when inedible (wood stick) object was available in cage. Effect was stronger in sated state (N = 5, two-way RM ANOVA laser × internal state effect $F[2,8] = 14.7$, *p = 0.002). H. Frequency of biting food pellet induced by CeA = > PCRt optical activation, which was elicited more robustly in the sated state (N = 5, two-way RM ANOVA laser × internal state effect $F[2,8] = 7.8$, *p = 0.013). I. Frequency of fictive feeding induced by CeA = > PCRt optical activation when food pellets were available in cage. (Laser effect N = 5, $F[2,8] = 31.1$, *p < 0.001). J-M. VGat-*Cre* mice were transfected with the *Cre*-dependent depolarizing designer receptor in PCRt and ChR2 in CeA. Panels show z-scores corresponding to electromyogram activity evoked by optical stimulation of CeA = > PCRt projections after administration of saline in masseter (J), (blue) and trapezius (K), (red) and after administration of designer drug CNO in masseter (L), (blue) and trapezius (M), (red). Z-scores were calculated as deviations from overall mean amplitude of the signal throughout a session. Shaded blue areas represent laser on period. Thick lines denote across-animals mean and thin lines the corresponding standard error of mean. The data reveal that administering the designer drug CNO completely abolished the ability of CeA to synergize the masseter and trapezius muscles. Laser effects: J: N = 5, $p < 0.001$; K: $p < 0.001$; L: $p > 0.15$; M: $p > 0.11$. N. Animals as in J-M above, but for Fos expression analyses the laser source was on performed only on the right hemisphere. Note that CeA = > PCRt activation reduced Fos expression in PCRt produced by CNO administration. O. As in (N), *Left:* Fos expression pattern analysis laser effect N = 5, paired t test: $T[4] = 5.1$, *p = 0.007). *Right:* Same as before but for Fos expression pattern analysis for cells located outside PCRt, laser effect $p > 0.9$. Rectangles shown positions of optical fibers, blue filled area represents laser on. P. The stereotaxic plates display the spatial distribution of a total of 35 distinguishable labeled cell clusters in CeA after injection of the *Cre*-inducible rabies construct SADΔG-GFP(EnvA) into PCRt. Injections were performed for both VGat-ires-*Cre* (N = 3 mice, 21 clusters, shown as green dots) and VGlut2-ires-*Cre* (N = 3 mice, 14 clusters, shown as blue dots). No significant differences between cluster numbers between two strains were found $\chi^2(1) = 2.76$, $p = 0.1$. In another cohort of mice, the same analyses were performed after SADΔG-GFP(EnvA) injections into VL/L PAG. The plates also show the spatial location of 28 clusters. For VGat-ires-*Cre* (N = 3 mice, 13 clusters, shown as purple dots) and VGlut2-ires-*Cre* (N = 3 mice, 15 clusters, shown as red dots). No significant differences between cluster numbers between two strains were found $\chi^2(1) = 0.28$, $p = 0.6$. The numbers below plates indicate distance from bregma. Note absence of labeled cells in adjacent regions. Data reported as mean ± SEM.

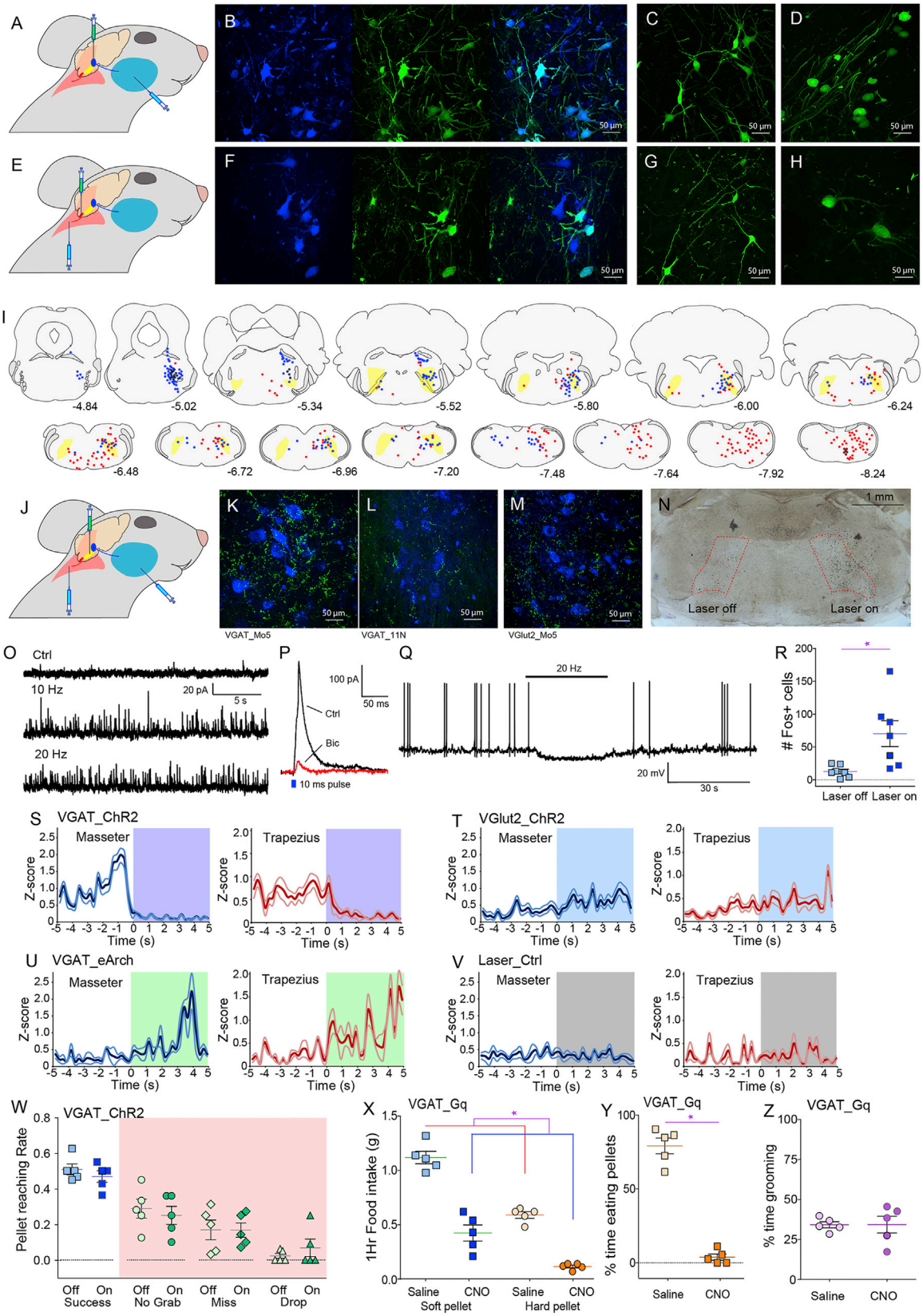

(legend on next page)

Figure S4. Premotor Circuits in the Parvocellular Reticular Formation, Related to Figure 4

A-D. The parvocellular reticular formation (PCRt) contains masseter (jaw-closing) premotor neurons. A. The retrograde dye FluoroGold was injected into the masseter concomitantly to injections of the *Cre*-dependent rabies construct SADΔG-GFP(EnvA) into the jaw-controlling motor trigeminal nucleus (Mo5) of Chat-ires-*Cre* × RΦGT mice. B. The resulting FluoroGold (blue), SADΔG-GFP(EnvA), and merged expressions in Mo5 are shown. The results confirm appropriate expression of SADΔG-GFP(EnvA) targeted Mo5. C. SADΔG-GFP(EnvA) labeled several Mo5-premotor cells in PCRt. D. Consistency with previous findings is supported by SADΔG-GFP(EnvA)-labeled premotor cells in the mesencephalic trigeminal nucleus. E-H. PCRt contains trapezius (head-orienting) premotor neurons. E. The retrograde dye FluoroGold was injected into the trapezius concomitantly to injections of the *Cre*-dependent rabies construct SADΔG-GFP(EnvA) into the neck-controlling accessory motor nucleus (11N) of Chat-ires-*Cre* × RΦGT mice. F. The resulting FluoroGold (blue), SADΔG-GFP(EnvA), and merged expressions in 11N are shown. The results confirm appropriate expression of SADΔG-GFP(EnvA) targeted 11N. G. SADΔG-GFP(EnvA) labeled several 11N-premotor cells in PCRt. H. Consistency with previous findings is supported by SADΔG-GFP(EnvA)-labeled premotor cells in the lateral vestibular nucleus. I. Representative mapping of jaw (N = 3 mice) and neck (N = 3 mice) premotor neurons superimposed on coronal sections of the mouse brain (Franklin & Paxinos, *The Mouse Brain in Stereotaxic Coordinates* 3rd ed., Elsevier, Amsterdam, 2008). Mo5-premotor cells labeled in blue, 11N-premotor cells labeled in red. Shaded yellow area delimits PCRt throughout the rostro-caudal sections. Coordinates shown with respect to bregma of adult (∼8weeks) male mouse. While the above injections of SADΔG-GFP(EnvA) in both Mo5 and 11N labeled a number of non-overlapping brainstem sites, only PCRt – and to a lesser extent the immediately adjacent intermediate reticular nucleus (IRt) – was found to contain premotor neurons to both Mo5 and 11N. We did not observe premotor cells labeled in regions outside the sections shown. J. The retrograde dye FluoroGold was injected into either the masseter or trapezius, concomitantly to injections of *Cre*-dependent synaptobrevin-fused eGFP into PCRt of either VGat-*Cre* or VGlut2-*Cre* mice. The panels suggest dense inhibitory contacts from PCRt onto motor neurons in both Mo5 (K) and 11N (L). Similar findings were obtained for excitatory glutamatergic contacts from PCRt onto motor neurons in both Mo5 (M) and 11N (not shown). N. Fos expression analyses based on the laser source activated only on the right hemisphere of VGat-*Cre* mice expressing *Cre*-dependent ChR2 in PCRt. Note selective increases in Fos expression on laser-stimulated hemisphere. Red-colored border delimits PCRt. Composite image across animals (N = 7) is shown. O. Representative traces show IPSCs of PCRt-ChR2-innervated vestibular neurons in control (0 Hz) and during 10 and 20Hz blue light stimulation conditions. Photostimulation of PCRt-ChR2 terminals in PCRt with 10 and 20Hz blue light significantly increased IPSC frequencies. The membrane potentials were held at −40 mV. P. Inhibitory postsynaptic current evoked by photostimulation of 10ms was inhibited by bicuculine (30 μM). Q. Representative trace shows that blue light at 20Hz clearly hyperpolarized and inhibited the targeted neuron. R. Fos expression analyses based on the laser source activated only on the right hemisphere of VGat-*Cre* mice expressing *Cre*-dependent ChR2 in PCRt (Composite image across animals shown in (N). Laser effect right versus left hemisphere N = 7 paired T-Test $t[6] = 3.4$, $^*p = 0.014$. S. VGat-*Cre* mice were transfected with the *Cre*-dependent ChR2 in PCRt. Panel shows z-scores corresponding to electromyogram activity evoked by optical stimulation of VGat neurons in PCRt in masseter. (left, blue) and trapezius (right, red). Z-scores were calculated as deviations from overall mean amplitude of the signal throughout a session. Shaded blue areas represent laser on period. Thick lines denote across-animals mean and thin lines the corresponding standard error of mean. The data reveal that optical stimulation of VGat neurons in PCRt rapidly and simultaneously flattened masseter and trapezius muscle signals. Laser main effect: both $p < 0.001$. T. Exactly same as in (S) but for VGlut2-*Cre* mice. The data reveal that optical stimulation of VGlut2 neurons in PCRt produce weak modulation of both masseter and trapezius (z-score change < 1.0, $p < 0.001$ for both muscles). U. Exactly same as in (S) but for eArch instead of ChR2 activation (green laser). The data reveal that optical inhibition of VGat neurons in PCRt rapidly and simultaneously induce greater activity in masseter and trapezius (z-score change > 2.0, $p < 0.001$ for both muscles). V. Same as before but laser source was off at all times. Events were the same randomly generated timestamps for laser activation during on sessions. No effects observed on either muscle (both $p > 0.1$). W. VGat-*Cre* mice were transfected with *Cre*-dependent ChR2 in PCRt. These mice were extensively trained on the pellet-reaching task, and on test sessions arm extension through the slit triggered the laser source. We observed no detrimental effects of PCRt activation on any of the performance parameters of the task, including overall success rate and other specific aspects of the task, such as failure to grab pellet, pellet misses, or pellet drops. N = 5, laser effect paired t test all $p > 0.12$. These results indicate that PCRt VGat photostimulation induces defects relatively specific to orofacial behaviors. X. VGat-ires-*Cre* mice were transfected with the *Cre*-dependent depolarizing designer receptor in PCRt. Administering the designer drug CNO strongly inhibited intake of both soft (high-fat) and hard (low-fat) food pellets (N = 5, two-way RM ANOVA main effect of CNO $F[1,4] = 74.5$, $^*p = 0.001$; CNO × pellet type $F[1,4] = 6.7$, $p = 0.06$). Y. This resulted from the treatment dramatically reducing the amount of time spent eating pellets (N = 5, $t[4] = 11.0$, $^*p < 0.001$). Z. However no general motor impairment was observed as grooming-like postures and movements were preserved after CNO administration (N = 5, $t[4] = 0.01$, $p = 0.9$). Data reported as mean ± SEM.

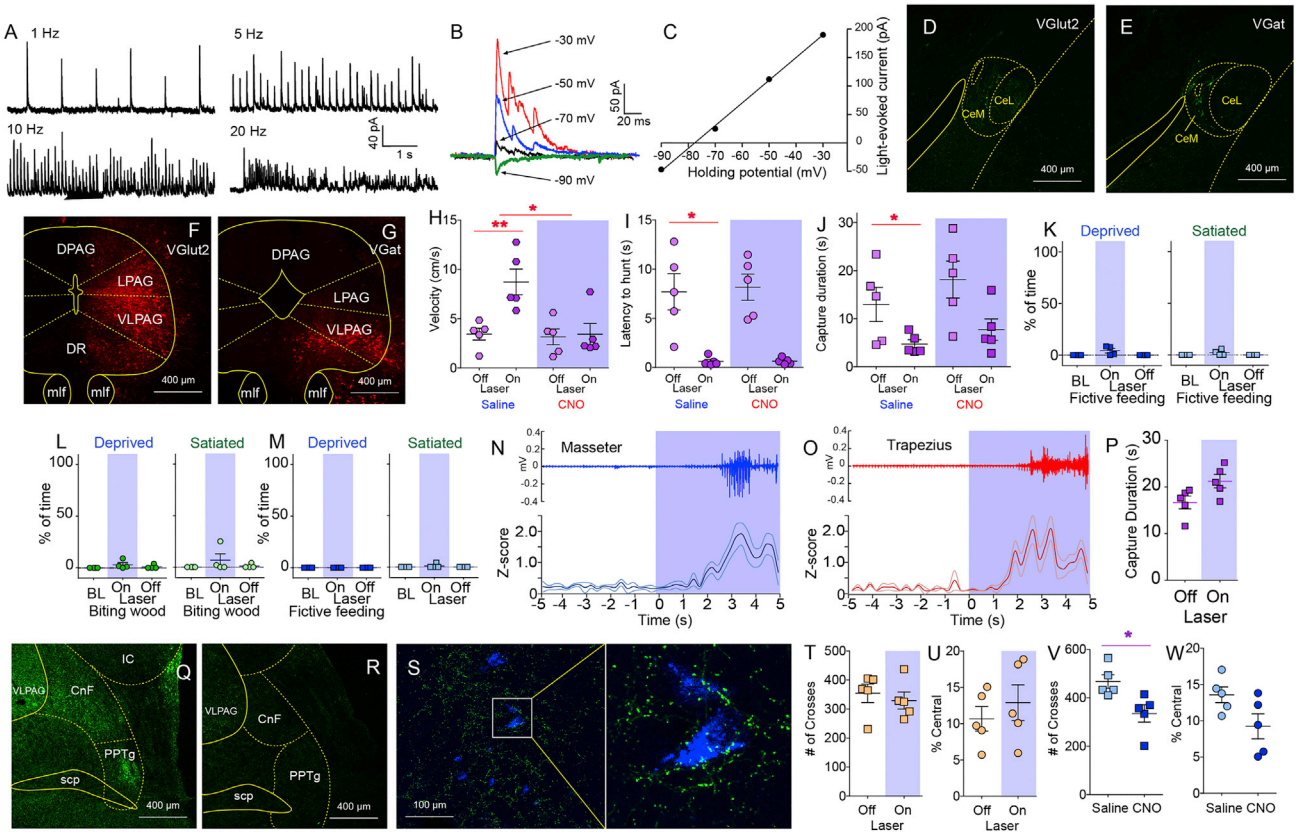

Figure S5. Central Amygdala Targets in Periaqueductal Gray, Related to Figure 5

A. Photostimulation (blue light at 1-20 Hz) of ChR2-expressing CeA neuronal terminals in PAG evoked outward postsynaptic currents in PAG neurons at the membrane potential of −40 mV. B. Photostimulation with 20ms blue light evoked postsynaptic currents in PAG neurons at holding potentials from −90mV to −30mV. C. Reversal potential of photostimulation-evoked postsynaptic current was obtained by linear current-voltage relationship. The Reversal potential is close to equilibrium potential for Cl^- current, revealing the characteristics of GABAergic postsynaptic Cl^- currents. D-E. *Cre*-dependent pseudotyped rabies virus SADΔG-GFP(EnvA) was injected in PAG of VGlut2-ires-*Cre* (D) and VGat-ires-*Cre* (E) mice. The panel shows the extent of labeling in centromedial (CeM) and centrolateral (CeL) regions of CeA. The figures reveal that most rabies-labeled cells were located within CeM, although fewer but detectable cells were located in CeL. See detailed distribution on Figure S3, panel (P). Note the absence of labeled cells in neighboring regions. F. Coronal section shows *Cre*-dependent designer receptor-fused mCherry expression in PAG of VGlut2-ires-*Cre* mice. DPAG = dorsal PAG, VL/LPAG = ventrolateral/lateral PAG, DR = Dorsal raphe, mlf = medial longitudinal fasciculus. G. Coronal section shows restricted *Cre*-dependent designer receptor-fused mCherry expression in VLPAG of VGat-*Cre* mice, in contrast to the pattern observed in VGlut2-*Cre* mice (F), where dense expression is observed in both VL and LPAG. H-J. Optical activation of CeA = > PAG projections elicited moderately faster prey pursuit (N = 5, paired t test **p = 0.04, panel (H), much shorter latencies to pursuit *p = 0.01, (I), and more efficient hunting *p = 0.04, (J). Chemogenetic activation of VGat-neurons in PAG caused a reduction in velocities (N = 5, two-way RM ANOVA CNO effect F[1,4] = 12.0, *p < 0.02). However, the CeA = > PAG enhancing effects on latencies (I) and capture duration (J) were not affected by CNO treatment (both F[1,4] < 2.2, p > 0.2). K-M. Optical stimulation of VGat CeA terminals in PAG, differently from terminals in PCRt, failed to induce fictive feeding in empty cages (K) or seizing/biting of inedible (wood sticks) objects (L) irrespective of internal state, or display fictive feeding in the presence of objects (M) in cage (N = 5, main effect of laser, all p > 0.1). N-O. VGat-ires-*Cre* mice were transfected with *Cre*-dependent ChR2 in CeA and optical fibers were implanted over PAG. Panels shows z-scores corresponding to electromyogram activity evoked by optical stimulation of VGat CeA terminals in PAG on masseter (N), (blue) and trapezius (O), (red). Z-scores were calculated as deviations from overall mean amplitude of the signal throughout a session. Shaded blue areas represent laser on period. Thick lines denote across-animals mean and thin lines the corresponding standard error of mean. The data reveal that optical stimulation enhanced masseter and trapezius muscle signals, albeit latency was conspicuously longer than for similar activation of CeA terminals in PAG. Laser effects: both p < 0.001. Importantly, latencies in electromyogram activity upon CeA = > PAG stimulation were much longer compared to CeA = > PCRt stimulation (masseter: 2.65 s ± 0.87 versus 0.69 s ± 0.45; trapezius: 2.45 s ± 0.90 versus 0.78 s ± 0.61 for CeA = > PAG versus CeA = > PCRt respectively, two-sample t test both p < 0.0001). Cf. Figures S3J and S3K for CeA = > PCRt data. P. Optical activation of CeA = > PCRt projections failed to alter hunting efficacy. No effects of laser were observed on duration of a successful hunting (p = 0.06). Q. *Cre*-dependent synaptobrevin-fused eGFP was virally transfected in VL/LPAG of VGlut2-*Cre* mice. Synaptobrevin expression reveals that VGlut2-neurons in VLPAG/LPAG project densely to the locomotion-controlling CnF and PPTg. CnF = Cuneiform nucleus, IC = Inferior colliculus, PPTg = pendunculopontine nucleus, scp = superior cerebral peduncle, VLPAG = Ventrolateral PAG. R. However, no projections from VGat-neurons in PAG were observed in MLR. S. A separate group of VGat-ires-*Cre* mice were injected with both the retrograde dye FluoroGold in MLR, and *Cre*-dependent synaptobrevin-fused eGFP into CeA. *Left:* Analyses of 40x confocal sections across VL/L PAG of these animals show abundant apposition of synaptobrevin-positive terminals onto MLR-projecting PAG neurons. *Right:* Magnified image of an MLR-projecting PAG neuron labeled with synaptobrevin terminals. T. Open field tests reveal no effects produced by optogenetic activation of PAG[VGlut2] = > MLR pathways on locomotor activity in a novel arena (number of crossings through the arena's subregions, N = 5, paired t test p = 0.4). U.

(legend continued on next page)

Neither were detected differences in time spent within the illuminated central area of the arena (p = 0.5). V-W. Open field tests revealed significant suppressing effects on locomotion produced by chemogenetic excitation of MLR neurons in a novel arena (number of crossings through the arena's subregions, N = 5, paired t test t[4] = 3.62, *p = 0.02). W. However, no differences were detected in time spent within the illuminated central area of the arena (p = 0.14). Data reported as mean ± SEM.

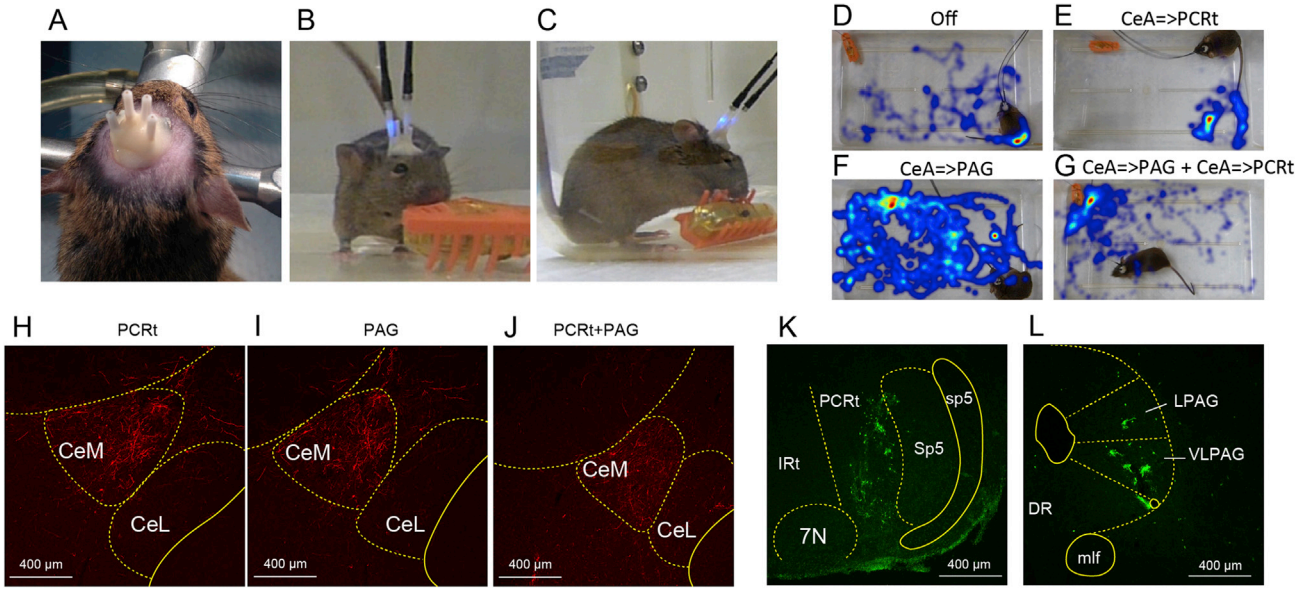

Figure S6. Simultaneous Activation of Central Amygdala Descending Pathways Terminating in Reticular Formation and Central Gray, Related to Figure 6

A. Outcome of the surgical approach to implant bilateral optical fibers above CeA terminals in both PAG and PCRt of VGat-ires-*Cre* mice. B-C. These same mice were transfected in CeA with *Cre*-inducible ChR2, and simultaneous unilateral stimulation of CeA = > PCRt and CeA = > PAG was employed. The pictures show an animal actively pursuing and attacking the artificial robot prey sustaining four optical fibers implanted on the skull. D-G. Illustrative locomotion heatmaps showing the patterns of artificial prey pursuit upon activation of the artificial robot prey when laser is off (D), CeA = > PCRt activation alone (E), CeA = > PAG activation alone (F), and CeA = > PCRt+CeA = > PAG combined activation (G). H. Wild-type mice were transfected with the retrograde CAV2-*Cre*-GFP construct into PCRt. CeA was then transfected with *Cre*-inducible ChR2-mCherry. The picture displays *Cre*-inducible expression of ChR2-mCherry in CeA. H. Wild-type mice were transfected with the retrograde CAV2-*Cre*-GFP construct into PCRt. CeA was then transfected with *Cre*-inducible ChR2-mCherry. The picture displays *Cre*-inducible expression of ChR2-mCherry in CeA of a mouse injected with CAV2-GFP-*Cre* in PCRt. I. Same as in (H) but for CAV2-*Cre*-GFP injections in PAG. J. Same as in (I) but for CAV2-*Cre*-GFP injections in PAG and PCRt. K-L. Example of injection site associated with CAV2-*Cre*-GFP injections in PCRt (K) and PAG (L). IRt = Intermediate reticular formation, 7N = (Facial) Motor nucleus VII, Sp5 = Spinal trigeminal nucleus, sp5 = spinal trigeminal tract, LPAG/VLPAG = Lateral/Ventrolateral PAG, DR = Dorsal raphe, mlf = medial longitudinal fasciculus.

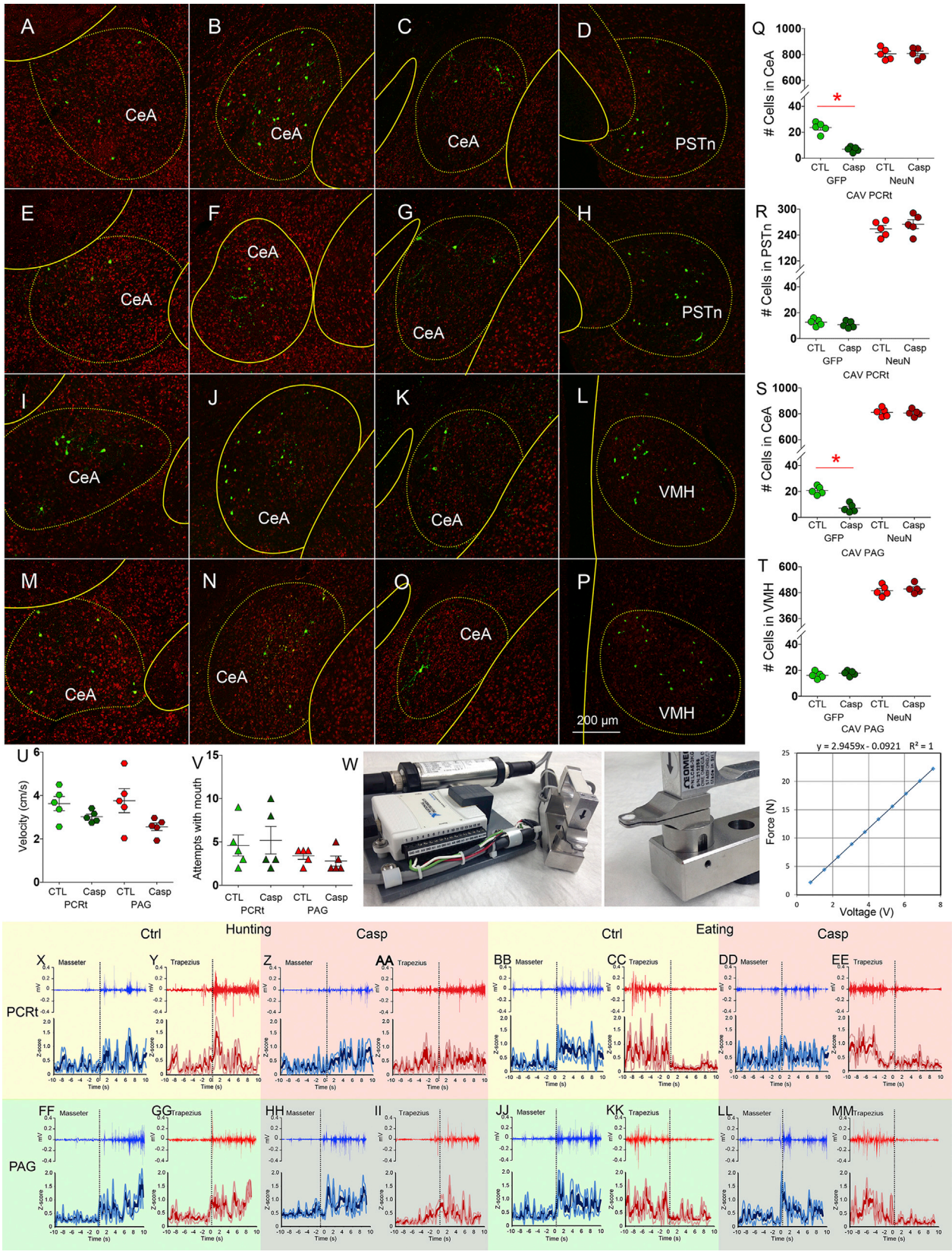

(legend on next page)

Figure S7. Analyses of Pathway-Defined Lesions in Central Amygdala, Related to Figure 7

Two different groups of wild-type mice were transfected with the retrograde CAV2-*Cre*-GFP construct into PCRt or PAG. CeA was then transfected with *Cre*-inducible AAV-caspase. Two groups of control mice were also injected CAV2-*Cre*-GFP construct into PCRt or PAG, but CeA then transfected with *Cre*-inducible AAV-mCherry. A-C. Confocal images of three different CeA levels after CAV2-*Cre*-GFP injections into PCRt of a PCRt-control mouse. D. Confocal image of the parasubthalamic nucleus of the hypothalamus (PSTN) after CAV2-*Cre*-GFP injections into PCRt of the same PCRt-control mouse. E-G. Confocal images of three different CeA levels after CAV2-*Cre*-GFP injections into PCRt of a CeA = > PCRt Caspase mouse. H. Confocal image of the PSTN after CAV2-*Cre*-GFP injections into PCRt of the same CeA = > PCRt Caspase mouse. I-K. Confocal images of three different CeA levels after CAV2-*Cre*-GFP injections into PAG of a PAG-control mouse. L. Confocal image of the ventromedial nucleus of the hypothalamus (VMH) after CAV2-*Cre*-GFP injections into PAG of the same PAG-control mouse. M-O. Confocal images of three different CeA levels after CAV2-*Cre*-GFP injections into PAG of a CeA = > PAG Caspase mouse. P. Confocal image of the VMH after CAV2-*Cre*-GFP injections into PCRt of the same CeA = > PCRt Caspase mouse. Q-T. Quantification of the effects of caspase lesions on each pathway. Q. CAV2-*Cre*-GFP injections into PCRt of CeA = > PCRt Caspase mice greatly reduced the number of detected GFP-positive cells on selected CeA slices compared to PCRt-control mice (N = 5 per group, two-sample t test t[8] = 8.2, Bonferroni *p < 0.008). No overall differences in NeuN expression were detected (p = 0.9). R. Similar analyses on selected PSTN slices revealed no group differences in either GFP or NeuN detection levels (both p > 0.3). S. CAV2-*Cre*-GFP injections into PAG of CeA = > PAG Caspase mice greatly reduced the number of detected GFP-positive cells on selected CeA slices compared to PAG-control mice (N = 5 per group, two-sample t test t[8] = 6.6, Bonferroni *p < 0.008). No overall differences in NeuN expression were detected (p = 0.8). T. Similar analyses on selected VMH slices revealed no group differences in either GFP or NeuN detection levels (both p > 0.5). U. Caspase ablation of the CeA = > PAG pathway only modestly affected pursuit velocities (N = 5 per group, two-way RM ANOVA lesion effect F[3,16] = 2.7, p = 0.07). V. Caspase ablation of the CeA = > PAG or CeA = > PCRt pathways failed to affect the total numbers of attempts to capture prey with mouth (N = 5 per group, F[3,16] = 12.8, p = 0.4). W. *Left* Apparatus used for measurement of biting forces. Values were obtained using an accurate single point load cell system (see *Experimental Procedures* for details). *Middle* The system was connected to a purpose-built, 3D-printed mouthpiece whose dimensions were based on incisor morphology of adult C57BL6/J mice. *Right* Linear calibration curve showing the output linear relation between voltage readings and actual force imposed on the mouthpiece. X. Electromyogram activity of masseter (left, blue) during hunting behavior in PCRt-control mice. The upper part shows a representative electromyogram trace and the lower part across-animal analyses (mean and corresponding standard errors). T = 0 was defined as initiation of hunting and the y axis displays the z-scores computed as deviations from the mean signal amplitude (z-score index for hunting versus pre-hunting baseline, Bonferroni p < 0.008). Y. Same as (X) but for trapezius (right, red, Bonferroni p < 0.008). Z-AA. In contrast, in CeA = > PCRt Caspase mice, masseter-trapezius coordination was affected as trapezius activity failed to increase during hunting (masseter, Bonferroni p < 0.008, Z; trapezius, Bonferroni p > 0.07, AA). BB-CC. Masseter activity increases and trapezius activity decreases during eating in control mice (masseter, Bonferroni p < 0.008, BB; trapezius, Bonferroni p < 0.01, CC). DD-EE. CeA = > PCRt Caspase mice masseter-trapezius coordination was affected as masseter activity failed to significantly increase during eating (masseter, Bonferroni p > 0.08, DD) although trapezius activity decreased as in controls (Bonferroni p < 0.008, EE). FF. Electromyogram activity of masseter (left, blue) during hunting behavior in PAG-control mice. The upper part shows a representative electromyogram trace and the lower part across-animal analyses (mean and corresponding standard errors). T = 0 was defined as initiation of hunting and the y axis displays the z-scores computed as deviations from the mean signal amplitude (z-score index for hunting versus pre-hunting baseline, Bonferroni p < 0.008). GG. Same as FF but for trapezius (right, red, Bonferroni p < 0.008). HH-II. Through plots HH-II. Same as in FF-GG, but for CeA = > PAG Caspase mice (all Bonferroni p < 0.008). JJ-MM. Same as in FF-II but for patterns recorded during eating (all Bonferroni p < 0.008). Data reported as mean ± SEM.